Imaging phenotyping of perivascular fat by computerised tomography detects human coronary inflammation

Alexios S. Antonopoulos[1]†, Fabio Sanna[1]†, Nikant Sabharwal[2], Sheena Thomas[1], Evangelos K Oikonomou[1], Laura Herdman[1], Marios Margaritis[1,3], Cheerag Shirodaria[2], Anna-Maria Kampoli[1], Ioannis Akoumianakis[1], Mario Petrou[4], Rana Sayeed[4], George Krasopoulos[4], Constantinos Psarros[1], Patricia Ciccone[1], Carl M. Brophy[1], Janet Digby[1], Andrew Kelion[2], Raman Uberoi[5], Suzan Anthony[5], Nikolaos Alexopoulos[6], Dimitris Tousoulis[6], Stephan Achenbach[7], Stefan Neubauer[1,3,8], Keith M Channon[1,3,8], Charalambos Antoniades[1,3,8]*

Affiliations:

[1]Division of Cardiovascular Medicine, Radcliffe Department of Medicine, University of Oxford, UK

[2]Cardiothoracic Directorate, Oxford University Hospitals NHS Foundation Trust, Oxford, UK

[3]Oxford Centre of Research Excellence, British Heart Foundation, UK

[4]Department of Cardiothoracic Surgery, Oxford University Hospitals NHS Foundation Trust, Oxford, UK

[5]Department of Radiology, Oxford University Hospitals NHS Foundation Trust, Oxford, UK

[6]Athens University Medical School, 1st Department of Cardiology, Greece

[7]Medizinische Klinik 2, Universitätsklinikum Erlangen, Erlangen, Germany

[8]Oxford Biomedical Research Centre, National Institute of Health Research, UK

†Contributed equally to the study;

Word count: 8,571 (main text)

Corresponding author: Prof Charalambos Antoniades MD PhD, Associate Professor of Cardiovascular Medicine, Division of Cardiovascular Medicine, University of Oxford, John Radcliffe Hospital, Oxford OX3 9DU, United Kingdom, Tel: +44-1865-228340, Fax: +44-1865-740352, e-mail: antoniad@well.ox.ac.uk

Abstract: Early detection of vascular inflammation is a long-standing goal that would allow deployment of targeted strategies for the prevention or treatment of multiple disease states. Since vascular inflammation is not detectable with commonly used imaging modalities, we hypothesized that phenotypic changes in perivascular adipose tissue (PVAT) induced by vascular inflammation could be quantified using a new computerized tomography angiography (CTA) methodology. We show that inflamed human vessels release cytokines that prevent lipid accumulation in PVAT-derived preadipocytes in vitro, ex vivo and in vivo. We developed a 3D PVAT analysis method and studied CT images of human adipose tissue explants from 453 patients undergoing cardiac surgery, relating the *ex vivo* images with *in vivo* CT scan information on the biology of the explants. We have developed a new imaging biomarker, CT Fat attenuation index (FAI), that describes adipocyte lipid content and size. FAI has excellent sensitivity and specificity for detecting tissue inflammation as assessed by tissue uptake of ^{18F}FDG in positron emission tomography (PET). In a validation cohort of 273 subjects, the FAI gradient around the human coronary arteries identified early subclinical coronary artery disease in vivo, and detected dynamic changes of PVAT in response to variations of vascular inflammation, and inflamed, vulnerable atherosclerotic plaques during acute coronary syndromes. Our study revealed that human vessels exert paracrine effects on the surrounding PVAT, affecting local intracellular lipid accumulation in preadipocytes, which can then be monitored using a CT imaging approach. This methodology can be implemented in clinical practice to allow the non-invasive detection of unstable plaques in the human coronary vasculature.

Key words: atherosclerosis; cardiovascular disease, adipose tissue; computerised tomography

Introduction

Inflammation is a key feature in atherogenesis (*1*) and modalities that can accurately detect vascular inflammation would enable better cardiovascular risk stratification and implementation of appropriate preventive strategies. Inflammation also characterizes vulnerable atherosclerotic plaques, the rupture of which leads to major cardiovascular events such as acute coronary syndromes and ischaemic strokes (*1*). Non-invasive detection of vascular inflammation has been hailed as the "holy grail" in cardiovascular medicine, as it would allow identification of patients at high risk for future cardiovascular events and initiation of appropriate risk reduction strategies. Current tools to assess vascular inflammation that rely on systemic plasma biomarkers (high sensitivity C-reactive protein, pro-inflammatory cytokines) are not directly related to the process of atherogenesis, do not identify vulnerable atherosclerotic plaques, and provide very poor associations with local vascular biological processes (*2*, *3*). Moreover, existing invasive (intravascular ultrasound, optical coherence tomography) and non-invasive [computerized tomography (CT) angiography or 18F-fluorodeoxyglucose (^{18F}FDG)-positron emission tomography–(PET)] imaging tools cannot provide reliable information on vascular inflammation in human coronary arteries (*4*). Coronary calcium scoring (CCS) is the only established non-invasive imaging biomarker with predictive value in primary prevention (*5*), but it describes non-reversible structural changes of the vascular wall, and it is not altered by interventions that reduce cardiovascular risk such as statins. An imaging biomarker that could overcome these limitations and non-invasively detect vascular inflammation would be invaluable in clinical research, risk stratification of coronary artery disease (CAD) and identification of patients at high risk of future cardiovascular events (*6*).

Adipose tissue releases a wide range of bioactive molecules that exert endocrine and paracrine effects on the vascular wall (*7*), and we have recently shown that the communication between adipose tissue and the vascular wall is bi-directional (*3, 8*). The biological properties of adipose tissue are largely driven by the degree of differentiation of small, immature preadipocytes to large, well-differentiated adipocytes, rich in intracellular lipid droplets (*9*). The differentiation of immature preadipocytes is promoted by *PPAR-γ* activation, but this mechanism is suppressed by exogenous inflammation (*10*). Currently there is no established non-invasive method to monitor adipocyte lipid content in human adipose tissue, although the correlation between adipocyte size and the balance between the lipid and aqueous phases of adipose tissue (*11*) may lend itself to detection by imaging modalities such as CT. Hence information about composition of tissues could provide indirect information on adipocyte size, a concept that has not been explored.

We hypothesized that the phenotypic characterization of human adipose tissue could be accomplished in a non-invasive manner by using CT imaging to assess adipocyte lipid content, and that coronary PVAT would function as a sensor rather than a driver of coronary inflammation. We further hypothesized that if vascular inflammation prevents lipid accumulation in preadipocytes of PVAT through paracrine signaling mechanisms, it may also lead to changes in tissue composition that could be detectable by high-resolution CT angiography (CTA). This approach would therefore permit detection of both inflamed coronary arteries without atherosclerosis and vulnerable atherosclerotic plaques prone to rupture, which would have important ramifications for patient management.

Results

Characterizing adipocyte size and lipid content in different adipose tissue depots The study flow chart is presented in fig. S1. We first studied the phenotypic differences between epicardial (EpAT), thoracic (ThAT) and subcutaneous (ScAT) adipose tissue obtained from 453 patients undergoing cardiac surgery (Study Arm 1, table S1). EpAT and ThAT had smaller adipocytes and increased adipocyte number compared to ScAT (Fig. 1A-E). In a proof-of-principle experiment we demonstrated that maturation of adipocytes is directly linked to lipid accumulation and downregulation of preadipocyte secreted factor (pref-1) that inhibits adipogenesis (fig. S2), resulting in increased adipocyte size that can be reliably tracked by fatty acid binding protein-4 (*FABP4*) gene expression (Fig. 1F). Fat depots with larger adipocytes, such as ScAT, had higher *PPAR-γ* (an adipocyte early phase differentiation marker (*9*)) (Fig. 1G), CCAAT/enhancer binding protein (C/EBP) alpha *(CEBPA*, an adipocyte late phase differentiation marker (*9*)) (Fig. 1H) and *FABP4* (a marker of terminal adipocyte differentiation/mature adipocytes) gene expression (Fig. 1I). These findings confirmed the notion that the expression of *FABP4, CEBPA*, and *PPAR-γ* genes could be used as markers of adipocyte size (*12*).

Effects of vascular inflammation on intracellular lipid accumulation of preadipocytes in human pericoronary adipose tissue

Our recent studies in humans (*3, 8*) and additional evidence from animal studies (*13*) suggest that adipocytes in PVAT respond to pro-atherogenic processes in the underlying vascular wall that modify their biology. We assumed that inflammatory signals from the human arterial wall may diffuse into the PVAT to influence adipocyte lipid content by affecting biological processes such as adipocyte differentiation, proliferation and lipolysis (*14*). Since fresh samples of native human

coronary arteries are not easily obtained for research, we used aortic tissue harvested during coronary artery bypass grafting (CABG) surgery as our model. Aortic "buttons" obtained from the site of graft anastomosis on the ascending aorta from patients in Study Arm 2 (table S1) were cultured ex vivo for one week in the presence or absence of angiotensin II (100nM) to induce vascular inflammation (Fig. 2A). Exposure to angiotensin II for one week led to up-regulation of the pro-inflammatory cytokines *IL-6,TNF-α,* and *IFN-γ* in the aortic tissue (Fig. 2B). The tissue was then washed to remove angiotensin II and co-cultured with preadipocytes collected from the same patients, followed by induction of adipocyte differentiation to mature adipocytes using a well-established methodology (*15*). When co-cultured with aortic tissue that was pre-treated with angiotensin II, preadipocytes showed less intracellular lipid accumulation compared to preadipocytes cultured in the absence of aortic tissue, indicating slower differentiation to mature adipocytes; preadipocytes co-cultured with non-stimulated aortic tissue had an intermediate amount of lipid accumulation (Fig. 2C-F). This suggests that mediators released from the inflamed human vascular wall can exert paracrine effects on PVAT, altering its lipid content in part by preventing the differentiation of preadipocytes to mature adipocytes.

To explore whether inflammatory mediators produced in the vascular wall directly modify lipid accumulation in PVAT, we exposed human preadipocytes collected from PVAT to recombinant IL-6+TNF-α+IFN-γ and studied their differentiation in vitro. Exposure of preadipocytes to cytokines had an inhibitory effect on preadipocyte differentiation as observed visually over time (fig. S3) and led to lower intracellular accumulation of lipid droplets (Fig. 3A-E). The same cytokines also accelerated the proliferation of human preadipocytes, evaluated using the MTS cell proliferation assay (Fig. 3F). The impact of these cytokines on preadipocyte differentiation was confirmed by quantifying the expression of *PPARγ*, *CEBPA* and *FABP4* during

the differentiation time-course (Fig. 3G-I). These findings support the notion that vessel-derived inflammatory cytokines inhibit lipid accumulation in PVAT by inducing the proliferation and inhibiting the differentiation of human preadipocytes in a paracrine manner. Therefore, we hypothesized that non-invasive imaging tools, capable of monitoring these phenotypic changes of PVAT driven by the underlying vascular inflammation, could be used to identify vascular inflammation in human coronary arteries.

Evaluating adipocyte lipid accumulation using computerized tomography

The balance between the lipid and aqueous phases of adipose tissue depends on adipocyte size (*11*) with larger adipocytes having increased lipid content and increased expression of *FABP4* (Fig. 1 and fig. S2). Since the CT attenuation of adipose tissue reflects the balance between lipid and aqueous phases, we concluded that adipose tissue CT attenuation may serve as a marker of adipocyte size/adipose tissue lipid content. To explore whether the average CT attenuation of adipose tissue provides a marker of average adipocyte size/adipose tissue lipid content, we quantified the Fat Attenuation Index (FAI) in EpAT , ThAT and ScAT explants obtained from 453 patients undergoing cardiac surgery (Study Arm 1). Briefly, the FAI is the average attenuation (reduction in signal) of adipose tissue within a volume of interest as measured from reconstructed CT. There was an inverse association between FAI and the degree of adipocyte differentiation as defined by the expression of *CEBPA* and *FABP4* in the same samples (Fig. 4A-F and table S2). However, FAI in EpAT did not correlate with the gene expression of *CD68,* a marker of macrophage infiltration (rho=0.180, P=0.096), or the ratio of *CCR7* (macrophage marker of M1 polarization) / MRC1 (macrophage marker of M2 polarization) (rho= -0.173, P=0.109) (fig. S4). There was a weak but significant association between FAI in ScAT and ThAT explants and the

ratio of *CCR7/MRC1* gene expression in the same samples, (rho= 0.182, P=0.007 for ScAT and rho= 0.191, P=0.001 for ThAT), although there was no significant correlation between FAI and *CD68* gene expression either in ScAT (rho=-0.116, P=0.065) or ThAT (rho=-0.078, P=0.166), (fig S4).

In addition, there was an inverse association between FAI of adipose tissue explants and adipocyte size quantified by histology (Fig. 4G). Accordingly, we established that FAI may be used as a marker of the variation of adipocyte size/adipose tissue lipid content in different depots: the greater the adipocyte differentiation/size, the more lipophilic the content of the tissue, therefore the more negative the FAI. To address this hypothesis in vivo, CT scans were performed in 105 patients (from Study Arm 1), aiming to link in vivo scan data with those from adipose tissue explants imaged ex vivo. We observed a correlation between the FAI obtained in vivo and the respective FAI measured in the explants of the same tissue that had been obtained from these patients (fig. 4H,I and table S2).

To further validate the ability of FAI to estimate adipocyte lipid content in vivo, we correlated the in vivo FAI values for EpAT and ScAT from CT scans of the 105 patients in Study Arm 1 who also underwent a clinical CTA with the expression of adipocyte differentiation markers. We observed that in vivo FAI (table S2) was inversely related to the expression of both *CEBPA* (Fig. 5A,B) and *FABP4* (Fig. 5C,D) in the respective adipose tissue depots from these patients. FAI in EpAT (FAI_{EpAT}) in vivo was higher compared to FAI in ScAT (FAI_{ScAT}) in vivo (Fig. 5E), confirming that histologically demonstrated differences in differentiation status of adipose tissue depots led to respective differences in FAI in vivo. HOMA-IR, a marker of systemic insulin resistance that has been associated with increased adipocyte size (*16*), was negatively associated with FAI_{ScAT} in vivo, but not with FAI_{EpAT} (Fig. 5F), suggesting that systemic metabolic status is

linked to adipocyte lipid accumulation in isolated adipose tissue depots such as ScAT but not in epicardial or pericoronary adipose tissue. In addition to systemic insulin resistance, adipocyte lipid content was also affected by the extent of tissue infiltration by inflammatory cells such as activated macrophages. Indeed, there was an inverse correlation between *CCR7/MRC1* gene expression ratio and *CEBPA* expression in ScAT (Fig. 6A) but not EpAT (Fig. 6B). In line with this finding, *CCR7/MRC1* ratio was positively associated with FAI in ScAT but not in EpAT (fig. S4) suggesting that FAI can be used as a surrogate marker of adipose tissue inflammation in isolated adipose tissue depots such as ScAT, but not in EpAT where FAI seems to be regulated by local stimuli from the coronary arteries.

To further explore the ability of FAI to describe adipose tissue inflammation, we validated it against ^{18F}FDG uptake by adipose tissue using PET-CT imaging, which is the gold standard modality to non-invasively assess tissue inflammation in vivo (*4*). In a validation study undertaken in 40 subjects who had ^{18F}FDG PET-CT for a clinical indication, we assessed ^{18F}FDG uptake by ScAT using the PET images and FAI using the coupled CT images from the same scans. We observed a positive association between ^{18F}FDG uptake and FAI in ScAT (Fig. 6C), but there was no association between these two biomarkers in EpAT, a finding in line with the gene expression studies performed in the two adipose tissue depots. Importantly, FAI_{ScAT} had excellent diagnostic accuracy for adipose tissue inflammation (defined using the median ^{18F}FDG uptake as a cut-off, TBR=0.200). For a cut-off value of FAI_{ScAT}=113.3.HU high AT inflammation (TBR>0.200) was detected with sensitivity of 90% and specificity of 100% (Fig. 6D). Representative images from a subject with high FAI_{ScAT} / high ^{18F}FDG uptake in ScAT and a subject with low FAI_{ScAT} / low ^{18F}FDG uptake in ScAT are presented in Fig. 6E.

Visualizing the changes in adipocyte size / adipose tissue lipid content in coronary PVAT in vivo

To investigate the relationship between FAI and adipocyte lipid content around the human coronary arteries, we compared adipose tissue obtained immediately adjacent to the RCA with adipose tissue obtained 2 cm away from the RCA and not in proximity with any visible epicardial coronary branch, from patients undergoing CABG in Study Arm 2. We observed that the expression of *PPAR-γ*, *CEBPA* and *FABP4* was downregulated closer to the RCA (Fig. 7A-C), while there was no difference in the expression of inflammatory mediators within the tissue or macrophage infiltration and polarization (fig. S5). This was in line with the observed smaller adipocyte size in proximity to the RCA compared to an area 2 cm away from the vascular wall (fig. 7D). These observations confirmed our findings from the ex vivo and in vitro experiments, suggesting that paracrine inflammatory signals from the human coronary artery rather than autocrine signals from within the tissue prevent lipid accumulation in PVAT surrounding them, although these effects are less marked as the distance from the RCA increases, even in the absence of obstructive vascular disease. To examine whether we could track these morphological changes of PVAT in response to coronary inflammation by non-invasive CT imaging, we used imaging analysis tools developed for the purpose of the study (UK Intellectual Property Office, application number 1414496.8) to analyse the CTA images of a clinical cohort of 273 subjects in Study Arm 3 (156 with and 117 without significant coronary plaques). We quantified FAI around the proximal segment of the RCA in 3D cylindrical layers of 1 mm thickness, starting from the layer immediately adjacent to the vascular wall and moving up to 20 mm away from it (Fig. 7E-G). FAI_{PVAT} calculation was feasible in all 3 major epicardial coronary arteries, but the RCA was used as a model to validate our ex-vivo findings given the absence of major side branches and the ability

to define PVAT vs non-PVAT, as well as the abundant amount of adipose tissue surrounding RCA which can be easily harvested without major bleeding risk, in contrast to the other epicardial arteries. We observed a progressive decrease of FAI to more negative values as we moved away from the RCA, from PVAT to non-PVAT (Fig. 7H-I), where adipocytes are larger (Fig. 7D) and better differentiated (Fig. 7A-C). These findings suggest that the observed changes of FAI could detect the degree of vascular inflammation inside the human coronaries using a non-invasive approach in vivo.

Validating FAI against established imaging biomarkers and coronary atherosclerotic plaque burden

To validate FAI against established imaging biomarkers with known clinical predictive value, we quantified CCS in the RCA alone and the entire coronary vasculature, and atherosclerotic plaque burden in the proximal RCA in the 273 individuals of Study Arm 3 (table S3). The relationships between FAI and distance from the vascular wall were significantly ($p=0.001$) different in patients with coronary atherosclerosis compared to healthy individuals (Fig. 7I), showing lower FAI values close to the vascular wall of healthy individuals. FAI in PVAT (FAI_{PVAT}, defined as the average FAI within a distance from the perimeter of the vessel equal to the diameter of the vessel) varied between patients even in the absence of coronary plaques (representative examples fig. S6). There was also a significant ($p=0.001$) difference in FAI_{PVAT} between patients with and without CAD independent of the presence of obstructive RCA disease (fig. S7), while there was no difference in $FAI_{non\text{-}PVAT}$ (defined as the FAI of an adipose tissue layer of 1 mm thickness, 2 cm away from the vascular wall) between CAD and non-CAD groups (Fig. 8A). When we examined the relationship between fat volumes and coronary atherosclerosis, we observed that EpAT volume was associated

with total CCS, while PVAT volume around RCA was not associated with either the presence of CAD or the RCA calcium burden (fig. S8). There was a weak association between FAI_{PVAT} and total CCS or RCA CCS (fig. S9, A-B). To study whether the gradient of FAI from PVAT around the RCA to non-PVAT 20 mm away from the RCA provides additional information to FAI_{PVAT}, we calculated the Volumetric Perivascular Characterization Index ($VPCI=[100x(FAI_{PVAT}–FAI_{non-PVAT})/|FAI_{PVAT}|]$). This index should not be affected by systemic factors modifying global adipocyte size, but would be mostly driven by local stimuli. VPCI was weakly associated only with the calcium burden in RCA but not total CCS (fig S9, C-D). Neither FAI_{PVAT} nor VPCI were correlated with calcification volume in the underlying segment of the analysed RCA (Fig. 8B,C), suggesting that these imaging indices describe biological processes not directly related with local vascular calcium deposition. Importantly, both FAI_{PVAT} and VPCI were related to atherosclerotic plaque burden in the underlying RCA segment (Fig. 8D-E), a finding which was similar for all major epicardial coronary arteries (fig. S10, B-D). VPCI was superior to FAI_{PVAT} in identifying non-calcified (soft) atherosclerotic lesions in the underlying coronary artery (Fig. 8F) but of moderate diagnostic value (fig. S11), suggesting that the current definition of vulnerable plaques as those without calcium does not accurately reflect the biological processes related to plaque rupture such as coronary plaque inflammation. To examine whether FAI_{PVAT} is related to the presence of CAD (defined as >50% stenosis in any coronary artery) independently of CCS, we performed multivariable linear regression in Study Arm 3, which showed that FAI_{PVAT} and CCS were related to the presence of CAD independently of each other and independently of age, gender and other cardiovascular risk factors (table S4). Similarly, FAI_{PVAT} (but not total CCS in the entire coronary tree or CCS in the RCA) was positively related with atherosclerotic plaque burden of the RCA independently of age, gender and cardiovascular risk factors (table S4).

Exploring the capacity of FAI to detect vascular inflammation and vulnerable atherosclerotic plaques

To further investigate the ability of FAI to detect dynamic changes in PVAT in response to variations in vascular inflammation, we studied FAI_{PVAT} around culprit lesions in patients with acute myocardial infarction (MI) within the previous 72 hours. The CTA scans were performed immediately after percutaneous coronary intervention (PCI), where both culprit and obstructive non-culprit coronary lesions were treated in the same session. We observed that FAI_{PVAT} was increased by 8.76+/-2.87HU around the culprit lesion compared to FAI_{PVAT} proximal to the lesion (Fig. 8G). Because the CTA was performed after stent implantation in the culprit lesion, we then sought to examine whether the observed result was due to a possible artifact from the stent. As controls, we used the non-culprit lesions from the same patients where stent implantation was performed simultaneously with the culprit lesion, as well as stable patients who had received a coronary stent more than 3 months prior to the scan. An increase in delta[FAI_{PVAT}] was observed around ruptured culprit lesions compared to either the non-culprit lesions in acute-MI patients or lesions in stable CAD patients treated with a stent >3 months before the CTA (Fig. 8G); in the same patients, in a pooled analysis of all lesions, delta[FAI_{PVAT}] was significantly ($p<0.001$) increased around ruptured compared to stable plaques (Fig. 8H) and had high diagnostic accuracy for detecting these areas of vascular inflammation (Fig. 8I).

To examine whether FAI_{PVAT} around the culprit lesions of patients with recent MI changes over time, a subgroup patients from the same cohort (n=5) underwent further CTA 5 weeks post-MI. Patients with stable CAD (n=5) were also re-scanned 5 weeks after the first scan to act as a control group. There was a significant ($p=0.04$) reduction in FAI_{PVAT} around the edges of the culprit lesion

5 weeks after the event, while there was no change in FAI_{PVAT} around the stable atherosclerotic plaques (Fig. 8J). Representative examples of differences in FAI_{PVAT} around a culprit stented lesion, a non-culprit stented lesion, a non-treated plaque, and a stent are provided (Fig. 8K).

Discussion

In the current study we present a method for detecting coronary inflammation by characterizing the changes in pericoronary adipose tissue CT attenuation. In a large cohort of patients undergoing cardiac surgery, we demonstrate that the average attenuation of adipose tissue (FAI) is correlated with the expression of adipogenic genes and average adipocyte size, which is driven by intracellular lipid accumulation. We also show that the expression of adipogenic genes, the average adipocyte size and lipid accumulation in PVAT are all driven by paracrine inflammatory signals from the vascular wall and are highly influenced by the presence of vascular disease. Using imaging tools developed for this purpose, we provide evidence that these biological effects of vascular inflammation on PVAT can be tracked by analysing standard imaging sequences obtained during CTA. This concept is summarized in a schematic (Fig. 8L). Based on this approach we provide imaging phenotyping that describes the degree of coronary artery inflammation, discriminates ruptured from non-ruptured coronary atherosclerotic plaques during acute coronary syndromes, and describes coronary atherosclerotic plaque burden independently of CCS.

Adipose tissue contains adipocytes of varying sizes and differentiation status (*9*). Induction of adipocyte differentiation in the adipose tissue includes post-confluent mitosis and growth arrest of preadipocytes, which is essential for their subsequent differentiation to mature adipocytes. *PPAR-γ* and *CEBPA* are synergistically and cooperatively responsible for the early and intermediate phases of differentiation of preadipocytes and their subsequent entry into the terminal

differentiation phase to mature adipocytes (*9*). In this latter phase, mature adipocytes are characterised by the expression of adipocyte-specific genes, expression of lipogenic enzymes (such as *FABP4*) and by accumulation of intracellular lipids, the amount of which determines the adipocyte size (*17*). We (*18*) and others (*19*) have shown that there are differences in adipocyte size and tissue biology between different human adipose tissue depots. In this study we demonstrate that the average adipocyte size is smaller in human EpAT and ThAT compared to ScAT, partly due to the presence of larger populations of immature preadipocytes identified by the lower expression of *PPAR-γ*, *CEBPA* and *FABP4*, and possibly other ongoing biological processes such as inflammation-induced lipolysis (*14*).

It is widely accepted that the balance between the lipid and aqueous phases of adipose tissue is driven by adipocyte size, due to the accumulation of intracellular lipids in large, mature adipocytes (*11*). In this study we demonstrate that this balance between the lipid and aqueous phases of adipose tissue can be estimated using CTA, by determining the average attenuation coefficient within a pre-defined radiodensity window (-190 to -30HU) (*20*). Previously it has been suggested that fat attenuation of visceral and subcutaneous adipose tissue depots provides important information, independently of fat volume or classic risk factors, on cardiovascular risk prediction (*20, 21*). Now we demonstrate that the average attenuation of adipose tissue (FAI) measured either ex vivo in adipose tissue explants or in vivo in patients undergoing clinical CTA shows an inverse correlation with adipocyte size and the expression of adipogenic markers such as *FABP4*, driven by the variations in intracellular lipid accumulation. This imaging phenotyping allows not only the characterization of adipocyte size within each adipose tissue depot, but also the detection of differences between different depots. Furthermore, validation of FAI_{ScAT} against in vivo ^{18F}FDG uptake, visualized by PET imaging, suggests that FAI can be used to reliably

quantify adipose tissue inflammation, at least in isolated depots such as ScAT where adipocyte size is driven by the infiltration of activated macrophages, insulin resistance, or other local tissue biology. FAI may have major applications in endocrinology, as adipocyte size and adipose tissue inflammation are important features of metabolic syndrome, which at present can only be assessed using adipose tissue biopsies or PET/CT respectively.

In our recent studies (*3, 8*) we have demonstrated a constant, bi-directional communication between the human arterial wall and its surrounding PVAT, introducing the concept that reverse, "inside-to-outside" signals originating from the vascular wall can affect the biology of PVAT in a paracrine manner. A previous study in mice has also shown that endovascular wire injury induces *PPAR-γ*-mediated phenotypic changes in PVAT, dependent on vascular TNF-α expression (*13*). Based on these findings, we now postulate that vascular inflammation may release inflammatory mediators that induce *PPAR-γ*-mediated structural changes in the neighbouring PVAT. Our results show that the human arterial wall expresses proinflammatory cytokines, and the inflamed arterial tissue prevents lipid droplet formation in PVAT adipocytes in an ex vivo co-culture system, by interfering with the ability of human preadipocytes to differentiate, as well as by triggering their proliferation.

Vascular inflammation is a key feature in atherogenesis, as it precedes the formation of atherosclerotic plaques (*1*). Despite the importance of vascular inflammation as a therapeutic target (*22, 23*), there are no reliable biomarkers to identify patients with high coronary inflammatory burden, as circulating inflammatory biomarkers are not specific and imaging modalities offer information only on the structural changes of the vascular wall. Clinical association studies have previously shown that inflammation of PVAT around the coronary arteries is increased in the presence of atherosclerosis, and it was conventionally believed that PVAT exerts a detrimental

effect on the human coronaries, inducing atherogenesis (*24*, *25*). Attention was also focused on linking volume (*26*) or inflammatory status (*27*) of PVAT with the presence of atherosclerotic plaques, while recent studies from the Chow group (*28*) have also linked EpAT thickness with coronary microvascular function in patients with non-obstructive coronary artery disease, and EpAT volume with coronary calcification and presence of non-calcified plaques (*29*). However, if vascular inflammation sends paracrine signals to PVAT to prevent lipid accumulation in adipocytes (*3, 8, 13*), this could lead to increased FAI_{PVAT} around inflamed coronary arteries, potentially detectable in-vivo. Firstly, we have demonstrated that there is a gradient in adipocyte size and the expression of adipogenic genes (*FABP4, CEBPA* and *PPAR-γ*) moving from PVAT adjacent to the human coronary arteries to adipose tissue further away. Secondly, we developed new imaging tools that enabled us to analyse FAI_{PVAT} in sequential cylindrical layers around the human coronary arteries, showing a parallel shift of FAI_{PVAT} to more negative values moving away from the vascular wall, reflective of the increase in adipocyte size/adipose tissue lipid content. FAI_{PVAT} was positively related to total atherosclerotic plaque burden and the presence of non-calcified (inflamed) atherosclerotic plaques in the underlying coronary artery since it flags the pro-inflammatory stimulation of pericoronary adipose tissue as the result of vascular inflammation. Even more importantly, we demonstrate that FAI_{PVAT} is increased around ruptured coronary atherosclerotic plaques of patients scanned during the acute phase of MI after stenting, possibly also due to the contribution of inflammatory cells infiltrating the perivascular space (*30*), a phenomenon that starts to resolve 5 weeks after the event. This latter finding suggests that FAI_{PVAT} may be used to non-invasively detect vulnerable atherosclerotic plaques, thereby enabling the identification of high risk patients. Our findings imply that the previously reported (*20, 21*) negative associations of CT attenuation of visceral or subcutaneous adipose tissue with

cardiometabolic risk, are explained by the fact that FAI in these depots describes increased adipocyte lipid accumulation, therefore it can be driven by other cardiometabolic risk factors like visceral obesity and insulin resistance. On the contrary, FAI_{PVAT} is positively associated with atherosclerotic plaque burden, but not with systemic insulin resistance, suggesting that it is indeed driven by local inflammatory stimuli coming from the vascular wall, rather than systemic metabolic conditions like insulin resistance.

The main limitation of this study is the lack of data demonstrating a predictive value of these imaging biomarkers for clinical outcomes, which falls beyond the scope of this current work. Moreover, the absolute values of FAI need to be tested and validated across different CT scanners in different centres, before the biomarkers described in this study become clinical applications.

In conclusion, the existing biomarkers with predictive value in CAD such as CCS have major weaknesses given that they do not change with interventions that modify cardiovascular risk and they represent permanent structural changes in the vascular wall. To track vascular inflammation in early disease states, we now introduce the concept that inflammation in the human coronaries drives changes in the surrounding PVAT in a paracrine manner, leading to less perivascular lipid accumulation closer to the vascular wall. We then describe a method and metrics of imaging phenotyping (FAI_{PVAT} and VPCI) that enable reliable tracking of these changes in adipocyte lipid content/size around the human coronary arteries. Importantly, the ability of these imaging tools to describe coronary atherosclerosis is independent of any cardiovascular risk factor or other established imaging biomarkers. The FAI_{PVAT} and VPCI may enable early detection of vascular inflammation, and have the advantage of being dynamic (they alter with changes in vascular inflammation) which is a major advantage over CCS. We also provide a tool that enables non-invasive detection of vulnerable (highly inflamed) atherosclerotic plaques in the human

coronary arteries. This approach can be used to analyze historical CTAs that have previously been performed in patients for diagnostic purposes. If the potential prognostic value of this new imaging phenotyping approach of PVAT is confirmed in clinical studies with prospective follow-up then it could have a major impact on risk stratification and clinical management of individuals in both primary and secondary prevention.

Material and Methods

Study design

The objective of this study was to develop a methodology for the detection of vascular inflammation in human coronary arteries, by performing functional imaging of coronary perivascular adipose tissue using CT angiography. This study a) links molecular phenotyping of human perivascular adipose tissue with its CT imaging characteristics ex-vivo and in-vivo, b) develops a method that links CT attenuation of human adipose tissue with lipid accumulation and tissue inflammation c) develops a method that uses molecular phenotyping and CT attenuation of perivascular adipose tissue around the human coronaries, as a means to quantify vascular inflammation related with atherosclerotic disease burden and plaque vulnerability in clinical cohorts.

Study Arm 1 consisted of 453 patients undergoing cardiac surgery at the Oxford University Hospitals NHS Foundation Trust (table S1). Adipose tissue samples (ThAT n=417, ScAT n=374, EpAT n=264) were harvested during surgery for gene expression studies, histology and CT imaging as explants. A subgroup of 105 patients also underwent CTA in order to link the histological and biological characteristics of the adipose tissue biopsies with the imaging characteristics of the same adipose tissue depots in vivo and in vitro. Study Arm 2 included 45

patients undergoing CABG (table S1) for mechanistic experiments and PVAT phenotyping. Study Arm 3 included a clinical cohort of 273 patients who underwent diagnostic coronary CTA (table S3) to validate the findings generated from Study Arms 1 and 2 and translate them in a clinical setting. Study Arm 4 included 22 patients with CAD (table S3) undergoing CTA to assess whether FAI_{PVAT} can identify unstable coronary plaques.

The study was conducted according to Declaration of Helsinki principles and approved by the local Research Ethics Committee (Oxford REC C 11/SC/0140, Oxford REC C 15/SC/0545 and Hippokration Hospital ID 2.2.15/1654 for Study Arm 4 study).

Blood sampling and measurements of circulating biomarkers

Fasting venous blood samples were obtained from the patients in Study Arm 1 prior to cardiac surgery. Serum insulin was measured by chemiluminescent microparticle immunoassay and serum glucose by the hexokinase method using commercial kits (ABBOTT). Insulin resistance was defined by HOMA-IR, calculated using the formula (glucose x insulin)/405, with glucose measured in mg/dL and insulin in mU/L.

Imaging studies using Computerised Tomography and Positron Emission Tomography/ Computerised Tomography

Details on CT and PET/CT imaging studies of adipose tissue, PVAT and coronary plaque characterization are presented in the Supplemental Material. Technical considerations on the calculation of the new imaging biomarkers FAI_{PVAT} and VPCI are presented in fig.S12 Briefly:

Adipose tissue characterization by CT: Adipose tissue was defined as all voxels with attenuation between -190 and -30 Hounsfield Units (HU). Voxel attenuation histograms were plotted and the

Fat Attenuation Index (FAI) was defined as the average attenuation of the adipose tissue volume of interest (within the pre-specified window of -190 to -30 HU; see Supplemental material for further details).

PVAT characterization: Perivascular tissue around the right coronary artery (RCA) was segmented into 20 concentric cylindrical 1mm-thick layers, extending between the 1st and 6th cm from its ostium, and FAI was calculated for each layer. The FAI curves of adipose tissue were plotted against the radial distance from the outer vascular wall. see Supplemental material for further details)

FAI of PVAT (FAI_{PVAT}): FAI_{PVAT} was defined as the FAI of adipose tissue in a layer of tissue within a radial distance from outer coronary artery wall equal to the average diameter of the tracked RCA segment. Non-PVAT FAI ($FAI_{non\text{-}PVAT}$) was defined at the most distal concentric layer of adipose tissue from RCA wall. Volumetric Perivascular Characterisation Index (VPCI) was then calculated as the %change in FAI from PVAT (FAI_{PVAT}) to non-PVAT (2cm away from the RCA's outer wall, $FAI_{non\text{-}PVAT}$), as defined above ($VPCI=[100x(FAI_{PVAT}–FAI_{non\text{-}PVAT})/|FAI_{PVAT}|]$); see Supplemental material for further details.

Coronary plaque analysis using CTA: Coronary plaques between 65-265 HU were defined as fibrous and >465HU as calcified. Atherosclerotic plaque burden was calculated as the ratio of fibrous plaque volume to total vessel volume (see Supplemental material for further details).

Statistical analysis

Continuous variables were tested for normal distribution using the Kolmogorov-Smirnov test. Non-normally distributed variables are presented as median [25th-75th percentile] and whiskers (Tukey). Normally distributed variables are presented as mean±SEM. Between groups

comparisons of continuous variables were performed using unpaired t-test (for 2 groups) or one-way ANOVA (or Kruskal-Wallis as appropriate) for 3 groups followed by Bonferroni (or Dunn's) post-hoc correction for multiple comparisons, as indicated. Paired comparisons were performed using paired t-test (or Wilcoxon signed rank test), and for 3 or more groups repeated measures ANOVA (or Friedman's test as appropriate). For between-group serial changes, we used two way ANOVA for repeated measures with interaction terms as presented in the Figure legends. Categorical variables were compared by using chi-square test. Correlations between continuous variables were assessed by using bivariate analysis, and Pearson's r or Spearman's rho coefficient was estimated as indicated in the figure legends.

To test whether FAI_{PVAT} is related with the presence of CAD we performed multivariable logistic regression for predictors of obstructive CAD (>50% stenosis of the lumen) and multivariate linear regression for atherosclerotic plaque burden in the RCA (independent variables as described in relevant text sections and Table S4). The results of the regression analysis are presented as standardized beta and P values. All statistical tests were performed using SPSS v20.0 and $P<0.05$ was considered statistically significant.

List of Supplementary Materials

Detailed Material and Methods

fig. S1. Study flow chart.

fig. S2. Adipocyte differentiation in-vitro and lipid accumulation

fig. S3. Effects of pro-inflammatory cytokines on preadipocyte differentiation

fig. S4. Fat Attenuation Index (FAI) and macrophage infiltration and polarization status in adipose tissue explants

fig. S5. Gene expression of inflammatory cytokines and markers of macrophage infiltration/ polarization in coronary perivascular vs non-perivascular adipose tissue.

fig. S6. Variation in Fat Attenuation Index (FAI) mapping of pericoronary adipose tissue in the absence of vascular disease.

References

1. R. Ross, Atherosclerosis--an inflammatory disease. *The New England journal of medicine* **340**, 115-126 (1999).
2. R. Lee, M. Margaritis, K. M. Channon, C. Antoniades, Evaluating oxidative stress in human cardiovascular disease: methodological aspects and considerations. *Current medicinal chemistry* **19**, 2504-2520 (2012).
3. M. Margaritis, A. S. Antonopoulos, J. Digby, R. Lee, S. Reilly, P. Coutinho, C. Shirodaria, R. Sayeed, M. Petrou, R. De Silva, S. Jalilzadeh, M. Demosthenous, C. Bakogiannis, D. Tousoulis, C. Stefanadis, R. P. Choudhury, B. Casadei, K. M. Channon, C. Antoniades, Interactions between vascular wall and perivascular adipose tissue reveal novel roles for adiponectin in the regulation of endothelial nitric oxide synthase function in human vessels. *Circulation* **127**, 2209-2221 (2013).
4. T. Christen, Y. Sheikine, V. Z. Rocha, S. Hurwitz, A. B. Goldfine, M. Di Carli, P. Libby, Increased glucose uptake in visceral versus subcutaneous adipose tissue revealed by PET imaging. *JACC. Cardiovascular imaging* **3**, 843-851 (2010).
5. P. Greenland, L. LaBree, S. P. Azen, T. M. Doherty, R. C. Detrano, Coronary artery calcium score combined with Framingham score for risk prediction in asymptomatic individuals. *JAMA* **291**, 210-215 (2004).
6. I. E. Hoefer, S. Steffens, M. Ala-Korpela, M. Back, L. Badimon, M. L. Bochaton-Piallat, C. M. Boulanger, G. Caligiuri, S. Dimmeler, J. Egido, P. C. Evans, T. Guzik, B. R. Kwak, U. Landmesser, M. Mayr, C. Monaco, G. Pasterkamp, J. Tunon, C. Weber, E. S. C. W. G. Atherosclerosis, B. Vascular, Novel methodologies for biomarker discovery in atherosclerosis. *European heart journal*, (2015).
7. C. Antoniades, A. S. Antonopoulos, D. Tousoulis, C. Stefanadis, Adiponectin: from obesity to cardiovascular disease. *Obesity reviews : an official journal of the International Association for the Study of Obesity* **10**, 269-279 (2009).
8. A. S. Antonopoulos, M. Margaritis, P. Coutinho, C. Shirodaria, C. Psarros, L. Herdman, F. Sanna, R. De Silva, M. Petrou, R. Sayeed, G. Krasopoulos, R. Lee, J. Digby, S. Reilly, C. Bakogiannis, D. Tousoulis, B. Kessler, B. Casadei, K. M. Channon, C. Antoniades, Adiponectin as a link between type 2 diabetes and vascular NADPH oxidase activity in the human arterial wall: the regulatory role of perivascular adipose tissue. *Diabetes* **64**, 2207-2219 (2015).
9. J. M. Ntambi, K. Young-Cheul, Adipocyte differentiation and gene expression. *J Nutr* **130**, 3122S-3126S (2000).
10. J. Bassols, F. J. Ortega, J. M. Moreno-Navarrete, B. Peral, W. Ricart, J. M. Fernandez-Real, Study of the proinflammatory role of human differentiated omental adipocytes. *Journal of cellular biochemistry* **107**, 1107-1117 (2009).
11. M. DiGirolamo, J. L. Owens, Water content of rat adipose tissue and isolated adipocytes in relation to cell size. *Am J Physiol* **231**, 1568-1572 (1976).
12. C. Farnier, S. Krief, M. Blache, F. Diot-Dupuy, G. Mory, P. Ferre, R. Bazin, Adipocyte functions are modulated by cell size change: potential involvement of an integrin/ERK signalling pathway. *Int J Obes Relat Metab Disord* **27**, 1178-1186 (2003).
13. M. Takaoka, H. Suzuki, S. Shioda, K. Sekikawa, Y. Saito, R. Nagai, M. Sata, Endovascular injury induces rapid phenotypic changes in perivascular adipose tissue. *Arteriosclerosis, thrombosis, and vascular biology* **30**, 1576-1582 (2010).
14. R. W. Grant, J. M. Stephens, Fat in flames: influence of cytokines and pattern recognition receptors on adipocyte lipolysis. *American journal of physiology. Endocrinology and metabolism* **309**, E205-213 (2015).
15. M. J. Lee, Y. Wu, S. K. Fried, A modified protocol to maximize differentiation of human preadipocytes and improve metabolic phenotypes. *Obesity (Silver Spring)* **20**, 2334-2340 (2012).
16. N. Franck, K. G. Stenkula, A. Ost, T. Lindstrom, P. Stralfors, F. H. Nystrom, Insulin-induced GLUT4 translocation to the plasma membrane is blunted in large compared with small primary fat cells isolated from the same individual. *Diabetologia* **50**, 1716-1722 (2007).
17. M. R. Kazemi, C. M. McDonald, J. K. Shigenaga, C. Grunfeld, K. R. Feingold, Adipocyte fatty acid-binding protein expression and lipid accumulation are increased during activation of murine macrophages by toll-like receptor agonists. *Arteriosclerosis, thrombosis, and vascular biology* **25**, 1220-1224 (2005).
18. A. S. Antonopoulos, M. Margaritis, P. Coutinho, J. Digby, R. Patel, C. Psarros, N. Ntusi, T. D. Karamitsos, R. Lee, R. De Silva, M. Petrou, R. Sayeed, M. Demosthenous, C. Bakogiannis, P. B. Wordsworth, D. Tousoulis, S. Neubauer, K. M. Channon, C. Antoniades, Reciprocal effects of systemic inflammation and

brain natriuretic peptide on adiponectin biosynthesis in adipose tissue of patients with ischemic heart disease. *Arteriosclerosis, thrombosis, and vascular biology* **34**, 2151-2159 (2014).
19. C. Bambace, A. Sepe, E. Zoico, M. Telesca, D. Olioso, S. Venturi, A. Rossi, F. Corzato, S. Faccioli, L. Cominacini, F. Santini, M. Zamboni, Inflammatory profile in subcutaneous and epicardial adipose tissue in men with and without diabetes. *Heart and vessels* **29**, 42-48 (2014).
20. K. J. Rosenquist, A. Pedley, J. M. Massaro, K. E. Therkelsen, J. M. Murabito, U. Hoffmann, C. S. Fox, Visceral and subcutaneous fat quality and cardiometabolic risk. *JACC. Cardiovascular imaging* **6**, 762-771 (2013).
21. T. M. Abraham, A. Pedley, J. M. Massaro, U. Hoffmann, C. S. Fox, Association between visceral and subcutaneous adipose depots and incident cardiovascular disease risk factors. *Circulation* **132**, 1639-1647 (2015).
22. D. Tousoulis, C. Psarros, M. Demosthenous, R. Patel, C. Antoniades, C. Stefanadis, Innate and adaptive inflammation as a therapeutic target in vascular disease: the emerging role of statins. *Journal of the American College of Cardiology* **63**, 2491-2502 (2014).
23. A. S. Antonopoulos, M. Margaritis, R. Lee, K. Channon, C. Antoniades, Statins as anti-inflammatory agents in atherogenesis: molecular mechanisms and lessons from the recent clinical trials. *Current pharmaceutical design* **18**, 1519-1530 (2012).
24. S. N. Verhagen, M. P. Buijsrogge, A. Vink, L. A. van Herwerden, Y. van der Graaf, F. L. Visseren, Secretion of adipocytokines by perivascular adipose tissue near stenotic and non-stenotic coronary artery segments in patients undergoing CABG. *Atherosclerosis* **233**, 242-247 (2014).
25. S. N. Verhagen, F. L. Visseren, Perivascular adipose tissue as a cause of atherosclerosis. *Atherosclerosis* **214**, 3-10 (2011).
26. P. Maurovich-Horvat, K. Kallianos, L. C. Engel, J. Szymonifka, C. S. Fox, U. Hoffmann, Q. A. Truong, Influence of pericoronary adipose tissue on local coronary atherosclerosis as assessed by a novel MDCT volumetric method. *Atherosclerosis* **219**, 151-157 (2011).
27. M. Konishi, S. Sugiyama, Y. Sato, S. Oshima, K. Sugamura, T. Nozaki, K. Ohba, J. Matsubara, H. Sumida, Y. Nagayoshi, K. Sakamoto, D. Utsunomiya, K. Awai, H. Jinnouchi, Y. Matsuzawa, Y. Yamashita, Y. Asada, K. Kimura, S. Umemura, H. Ogawa, Pericardial fat inflammation correlates with coronary artery disease. *Atherosclerosis* **213**, 649-655 (2010).
28. M. S. Alam, R. Green, R. de Kemp, R. S. Beanlands, B. J. Chow, Epicardial adipose tissue thickness as a predictor of impaired microvascular function in patients with non-obstructive coronary artery disease. *J Nucl Cardiol* **20**, 804-812 (2013).
29. N. Alexopoulos, D. S. McLean, M. Janik, C. D. Arepalli, A. E. Stillman, P. Raggi, Epicardial adipose tissue and coronary artery plaque characteristics. *Atherosclerosis* **210**, 150-154 (2010).
30. E. Henrichot, C. E. Juge-Aubry, A. Pernin, J. C. Pache, V. Velebit, J. M. Dayer, P. Meda, C. Chizzolini, C. A. Meier, Production of chemokines by perivascular adipose tissue: a role in the pathogenesis of atherosclerosis? *Arteriosclerosis, thrombosis, and vascular biology* **25**, 2594-2599 (2005).

Acknowledgments: We are grateful to Dr Meisam Naeimi Kararoudi for his support in the analysis of part of the ex vivo images of adipose tissue explants.

Funding: The study was funded by the British Heart Foundation (FS/16/15/32047 and PG/13/56/30383 to CA) the BHF Centre of Research Excellence, Oxford (RE/08/004 to MM/CA), the National Institute for Health Research - Oxford Biomedical Research Centre, the European Commission (Marie Curie ITN RADOX GA316738 and IF REDO$_X$HEART GA656990) and the NovoNordisk Foundation (NNF15CC0018486).

Competing Interests: The method for analysis of perivascular Fat Attenuation Index (FAI) and the Volumetric Perivascular Characterization Index (VPCI) described in this manuscript is subject to a UK patent application, number 1414496.8.

Author Contributions: A.S.A participated in patient recruitment, clinical data and biological samples collection, data analysis, statistical analysis and writing of the manuscript; F.S., M.M, C.P., and P.C performed experiments, data analysis and reviewed the manuscript; N.S. participated in clinical data collection; S.T. participated in clinical data collection and data analysis; L.H. participated in patient recruitment and data analysis; I.A. performed experiments; C.S. participated in clinical data collection and reviewed the manuscript; E.O. participated in clinical data collection and image/data analysis; AM.K. and C.M.B participated in data analysis; M.P., R.S and G.K. contributed to participant recruitment and biological samples collection; A.K., R.U., S.A. N.A., D.T. contributed to clinical data collection; J.D., S.A., S.N. and K.M.C provided advice, discussed and reviewed the manuscript, C.A designed the study, raised the funding, coordinated and directed the project, and wrote the manuscript.

Data and materials availability: All data are included in the paper or the supplement. For any further information, please contact the corresponding author.

Figure Legends

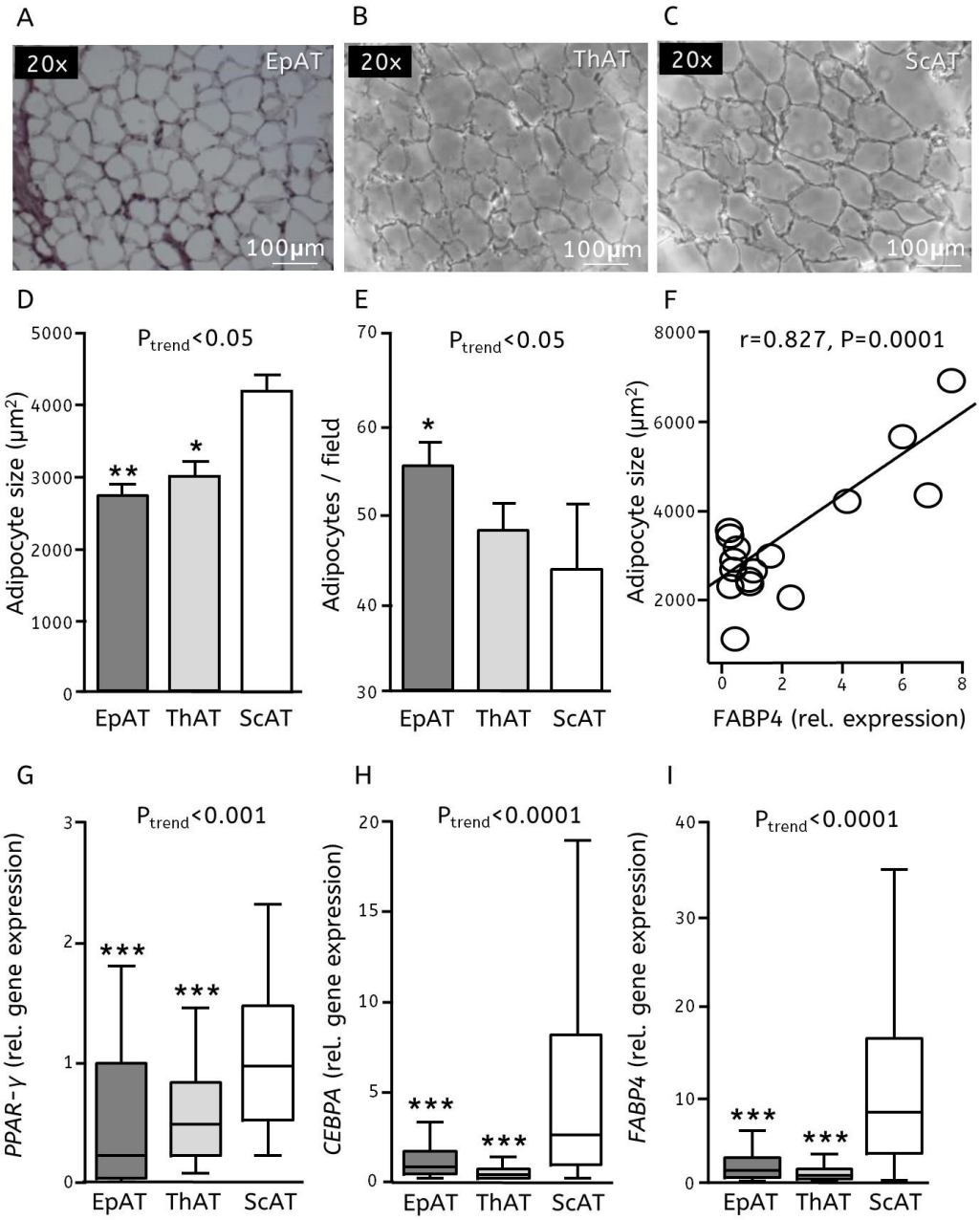

Fig. 1. Phenotyping of human adipose tissue. Representative bright field microscopic images of human **(A)** epicardial (EpAT), **(B)** thoracic (ThAT), and **(C)** subcutaneous (ScAT) adipose tissue. **(D)** Adipocyte size (n=5 patients) and **(E)** adipocytes per field (n=6 patients), quantified from tissue sections of EpAT, ThAT, and ScAT from the same patients. (**F**) Adipocyte size correlated with *FABP4* expression (n=16). (**G**) Gene expression of *PPAR-γ,* (**H**) *CEBPA* (**I**) *FABP4* (for G-I: samples from n=433 patients). P-trend derived from repeated measures ANOVA with Bonferroni correction (D), Friedman's test with Dunn's post-hoc correction (E) or Kruskal Wallis with Dunn's post-hoc correction (G-I) *P<0.05, **P<0.01 vs ScAT.

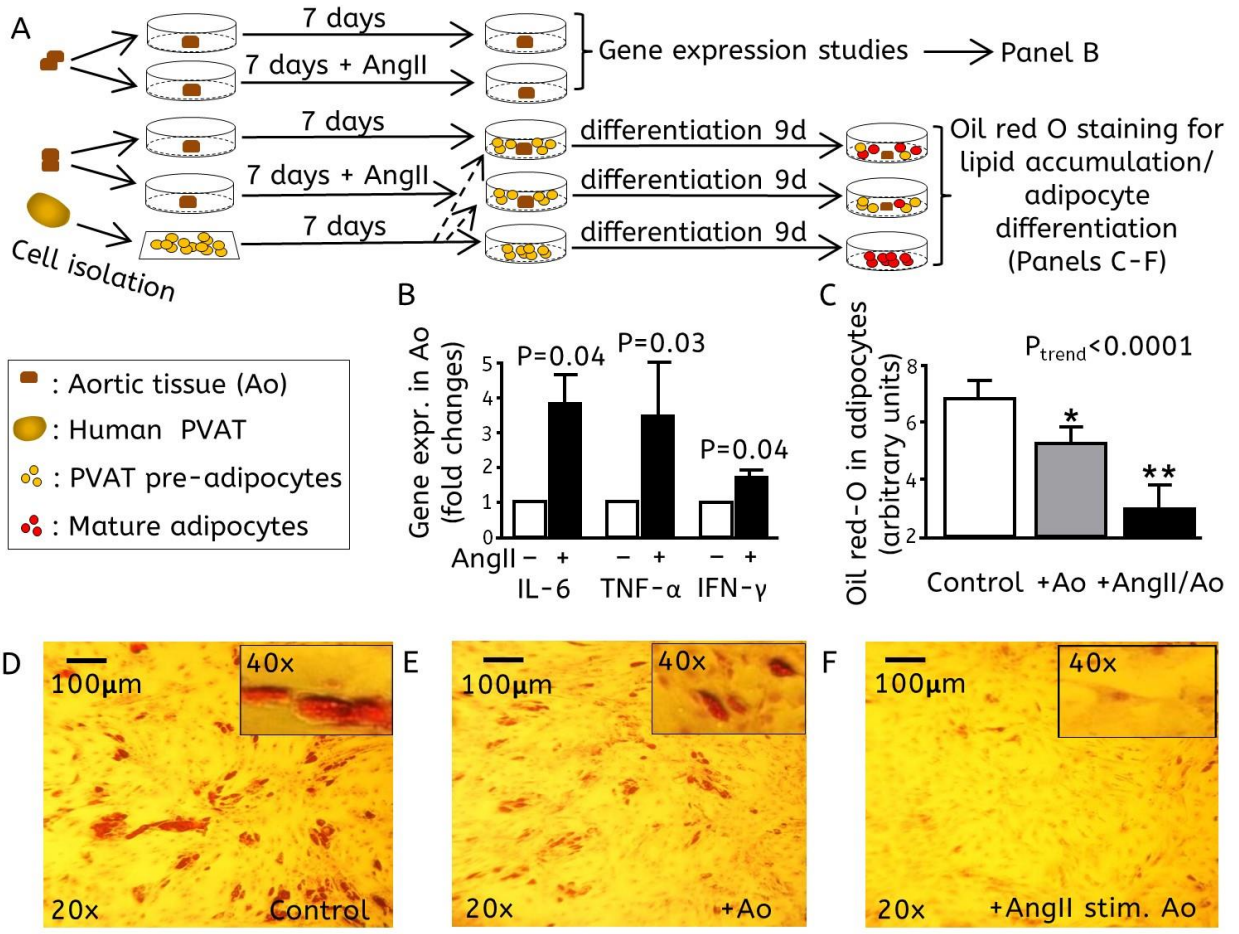

Fig. 2. Vascular inflammation blocks perivascular adipocyte differentiation through paracrine signals. (**A**) Experimental design of the co-culture experiments in Study Arm 2. Human aortic tissue (Ao) from 15 patients undergoing coronary artery bypass grafting was harvested and cultured for 7 days +/- angiotensin II (AngII, 100 nM). Preadipocytes isolated from PVAT around the RCA were also cultured for this period. After 7 days, the Ao was washed to remove AngII and was co-cultured with the preadipocytes before a differentiation time-course was induced. (**B**) *IL-6, TNF-α* and *IFN-γ* gene expression in Ao before and after stimulation with AngII (n=5-7 per group). (**C**) Quantification of oil red-O in pre-adipocytes (control) or pre-adipocytes co-incubated with Ao or Ao pre-stimulated with AngII (n=6 per group). **(D-F)** Representative images of oil red-O staining in pre-adipocytes co-incubated with Ao as in (C). P values derived from Wilcoxon signed rank test (B) and repeated measures ANOVA followed by-individual comparisons using paired t-test (C); *P<0.05, **p<0.001 vs control.

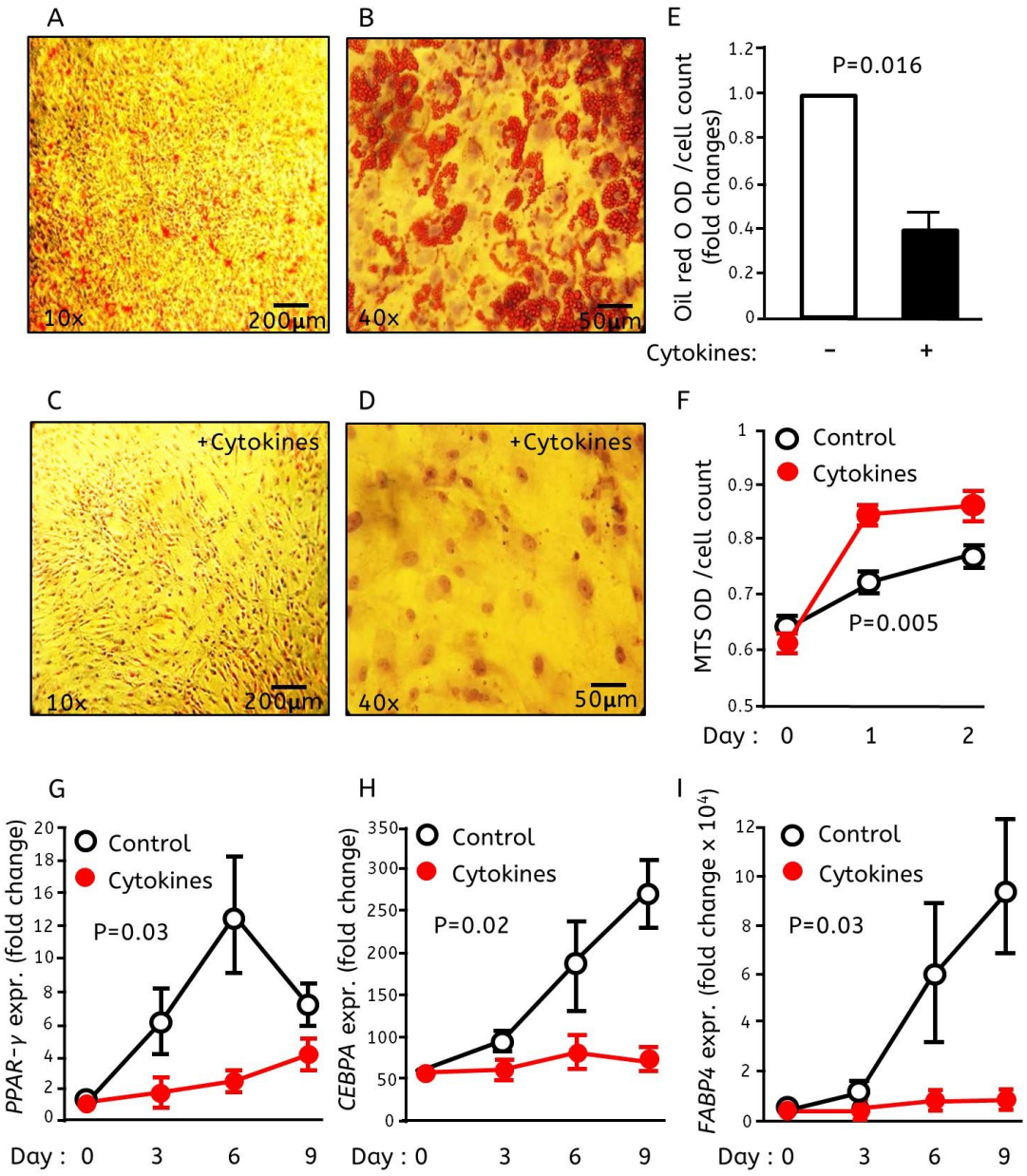

Fig. 3. Cytokines trigger proliferation and block differentiation of perivascular adipocytes. In Study Arm 2, human preadipocytes were isolated from perivascular adipose tissue (PVAT) around the right coronary artery and differentiated in the presence or absence of inflammatory cytokines [recombinant TNF-α (4 ng/ml) + IL-6 (25 ng/ml) + IFN-γ (20 ng/ml)] until day 9 of differentiation (**A-B** without cytokines and **C-D** with cytokines, oil-red-O staining at day 9 of differentiation). **(E)** Oil-red-O photometric quantification of lipid accumulation in preadipocytes differentiated with and without cytokines (n=7). Effects of cytokines on **(F)** preadipocyte proliferation and gene expression of the differentiation markers (**G**) *PPAR-γ*, (**H**) *CEBPA* and (**I**) *FABP4* (n=3 independent experiments in triplicate). P-values derived from Wilcoxon signed rank test (E) or two-way ANOVA with 'time x treatment' interaction (F-I).

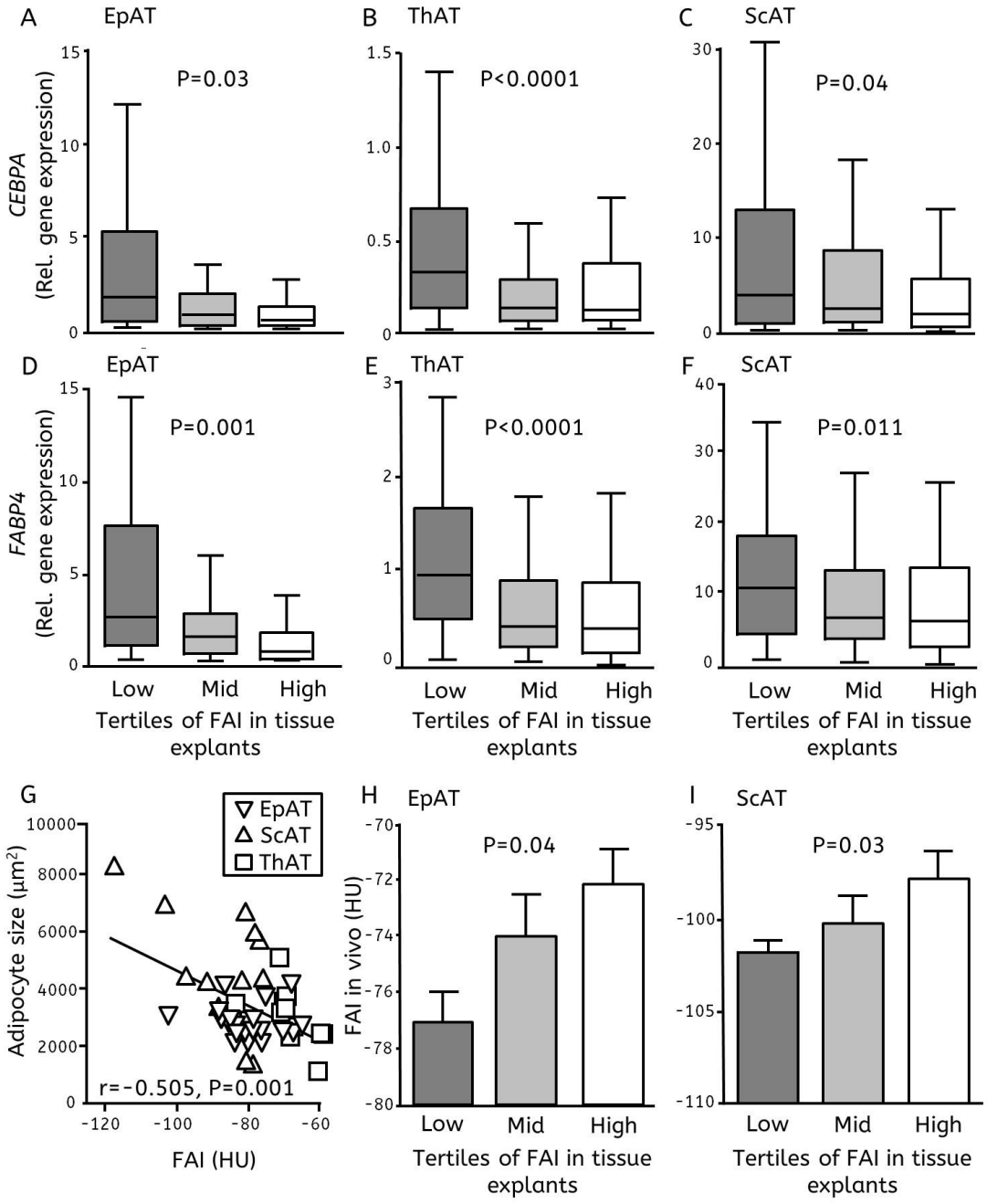

Fig. 4. Ex vivo characterization of adipocyte size and adipogenesis using CT. Explants of epicardial (EpAT), thoracic (ThAT) and subcutaneous (ScAT) adipose tissue from patients undergoing coronary-artery bypass grafting (Study Arm 1) were scanned by computerised tomography (CT) to calculate Fat attenuation index (FAI) for each sample. Association of FAI with the expression of (**A-C**) *CEBPA* (EpAT: n=87, ThAT: n=311, ScAT: n=288**)** and (**D-F**) *FABP4* (EpAT: n=85, ThAT: n=312, ScAT: n=259) genes in all depots. **(G)** Correlation between adipocyte size and FAI (n=44 biopsies). Association between FAI measured in vivo and in explants of (**H**) EpAT and (**I)** ScAT collected from 105 patients in Study Arm 1. p-values by Kruskal Wallis (A-F) and one-way ANOVA (H-I).

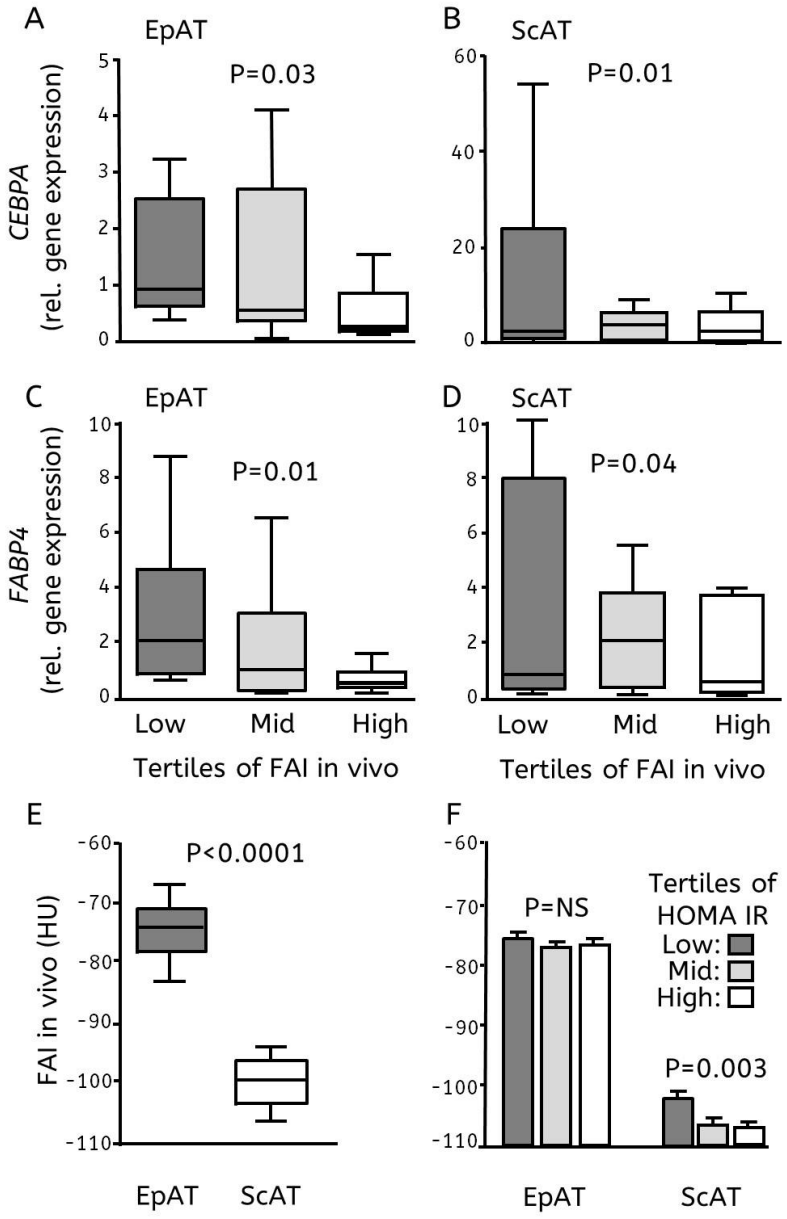

Fig. 5. In vivo characterization of adipogenesis by CT. Association of in vivo Fat attenuation index (FAI) for epicardial (EpAT) and subcutaneous (ScAT) adipose tissue of patients undergoing computerised tomography (CT) with gene expression of (**A-B**) *CEBPA* and (**C-D**) *FABP4* by the same adipose tissue samples collected from the same patients during surgery (Study Arm 1). (**E**) Comparison of in-vivo FAI between EpAT and ScAT and (**F**) associations with systemic insulin resistance. p-values by Kruskal Wallis (A-D) or Wilcoxon signed rank text (E) or one-way ANOVA (F). NS: Non-significant. Studies performed in the 105 patients from the in vivo CTA group of Study Arm 1.

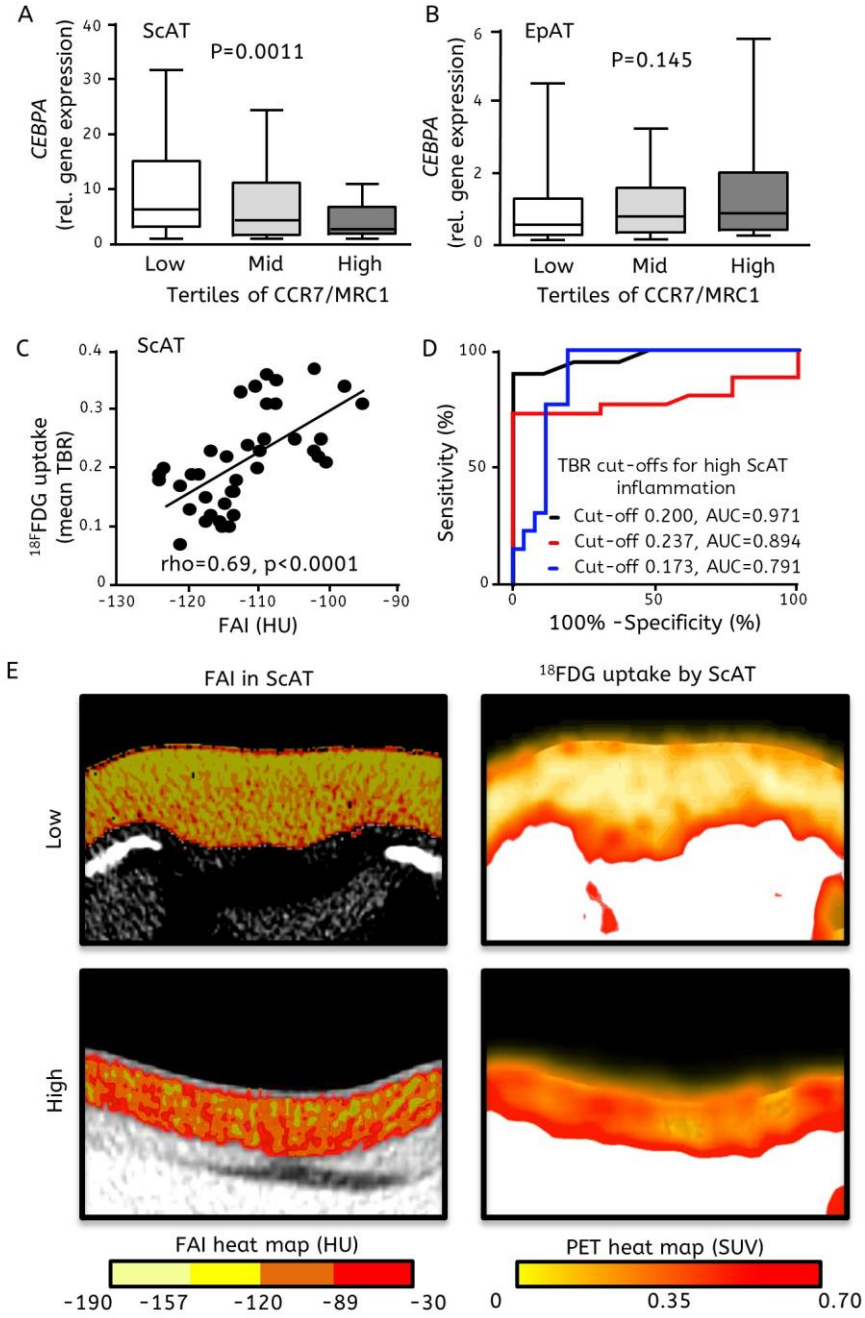

Fig. 6. Fat Attenuation Index (FAI) for the detection of human adipose tissue inflammation by non-invasive imaging. Associations between *CEBPA* gene expression and *CCR7/MRC1* gene expression ratio in (**A**) subcutaneous (ScAT, n=267) or (**B**) epicardial (EpAT, n=207) adipose tissue in Study Arm 1. (**C**) Correlations between ^{18F}FDG uptake of ScAT by positron emission tomography /computerized tomography (PET/CT, determined as the mean tissue to background ratio, TBR) with FAI of the same tissue (n=39) and (**D**) Receiver Operating Characteristic curves for identification of highly inflamed ScAT by FAI according to ^{18F}FDG uptake measured by PET/CT. (**E**) Representative examples of FAI and ^{18F}FDG uptake heat maps in ScAT. p-values by Kruskal Wallis test (A-B).

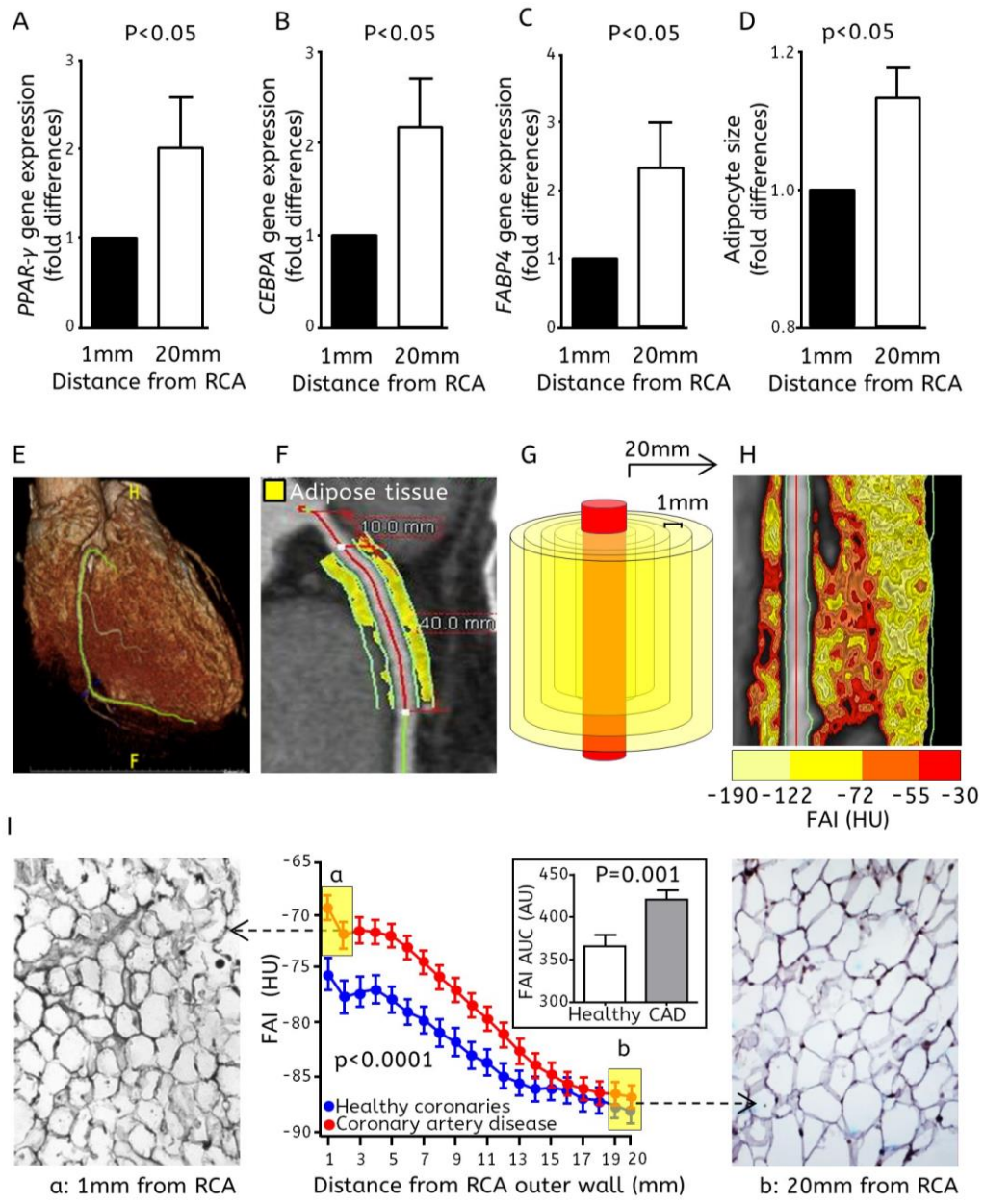

Fig. 7. Gradient of adipocyte size and Fat Attenuation Index (FAI) around the human coronaries in the presence or absence of coronary atherosclerosis. (A) *PPAR-γ*, (**B**) *CEBPA* and (**C**) *CEBPA4* gene expression and (**D**) adipocyte size in pericoronary adipose tissue samples attached to the right coronary artery (RCA) and paired samples ~20mm away from it (n=6-12 pairs for A-D). (**E-G**) In Study Arm 3, Fat attenuation index (FAI) around the RCA of patients undergoing CT angiography was calculated for each cylindrical 1 mm-thick layer of pericoronary tissue, for a radial distance from RCA wall 1 mm to 20 mm. (**H**) FAI mapping of PVAT around the RCA. (**I**) FAI and radial distance from vascular wall in patients with coronary artery disease (n=149) vs healthy individuals (n=117) (comparison of the area under the curve (AUC) using unpaired t-test and comparison of the curves using two-way ANOVA for repeated measures with 'FAI x distance' interaction. p-values by Wilcoxon signed rank test (A-D).

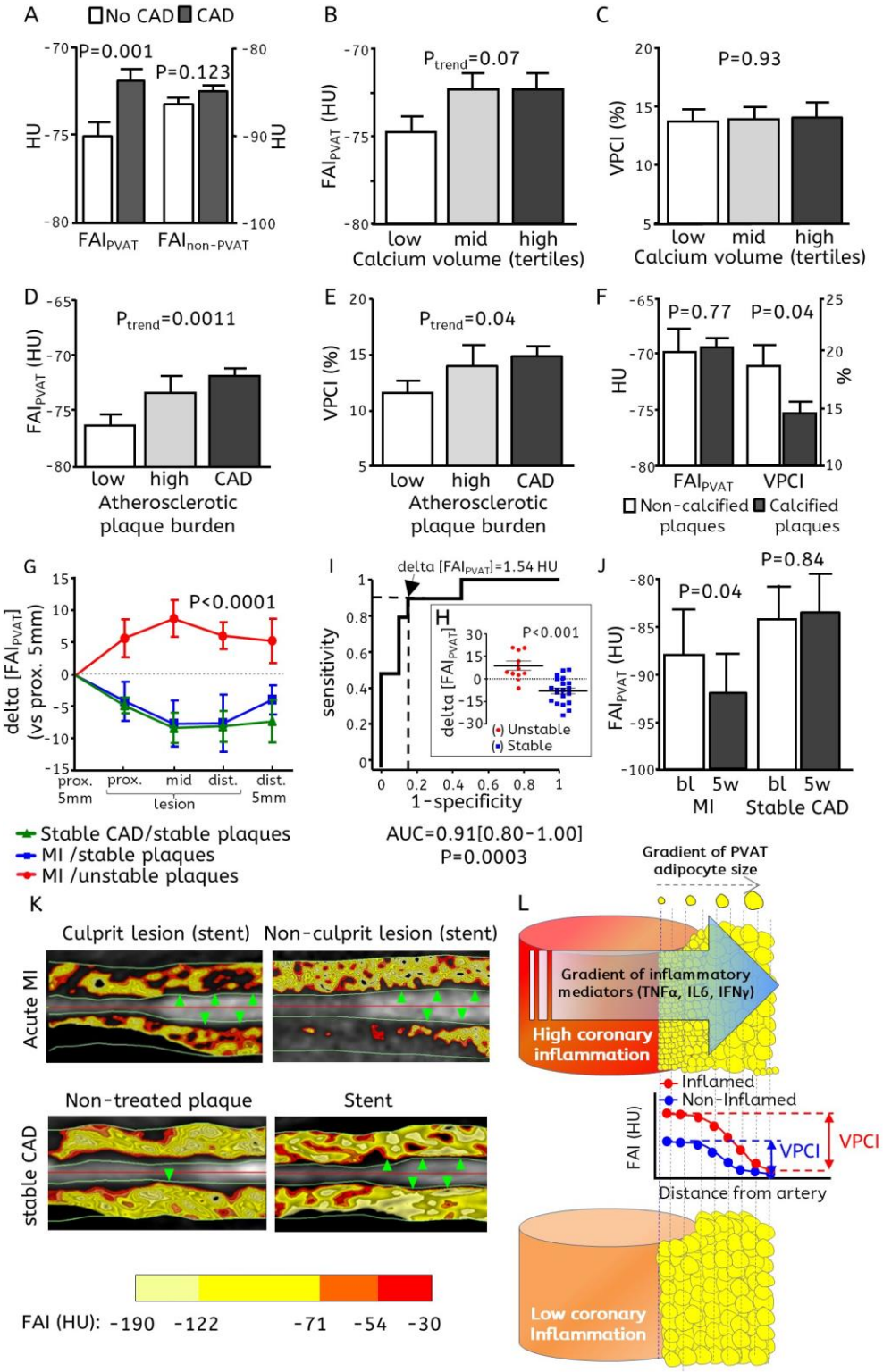

Fig. 8. FAI$_{PVAT}$ and VPCI as novel phenotyping tools for vascular disease. (A) Associations between FAI$_{PVAT}$/FAI$_{non-PVAT}$ and coronary artery disease (CAD). (**B-C**) Association between calcification volume and FAI$_{PVAT}$ or VPCI. (**D-E**) Both FAI$_{PVAT}$ and VCPI are related with atherosclerotic plaque burden in RCA (n=267 for panels A-E). **(F)** Comparisons of FAI$_{PVAT}$ and

VCPI between non-calcified plaques (n=26) and mixed or calcified plaques (n=84) in CAD patients with high atherosclerotic plaque burden in the RCA (defined as >33rd percentile). (**G**) Changes in FAI_{PVAT} around ruptured (culprit) atherosclerotic lesions (n=10) of acute myocardial infarction (MI) patients, non-culprit lesions of the same patients (n=7) or lesions in stable CAD patients (n=13); delta[FAI_{PVAT}]= $FAI_{PVAT(around\ lesion)}$ –$FAI_{PVAT(proximal\ segment}$. (**H**) Comparison of delta[FAI_{PVAT}] between stable and unstable plaques and (**I**) its diagnostic accuracy in receiver operator characteristic (ROC) curve analysis for detection of unstable plaques (culprit lesions). (**J**) Paired CT scans with 5 weeks difference, to assess temporal changes of FAI_{PVAT} in acute MI and stable CAD patients (n=5). (**K**) Representative images of FAI_{PVAT} colour maps around: 1) a culprit lesion (green arrowheads, identified by the presence of the stent, upper left image) 2) a non-culprit lesion from the same patient (identified by the presence of the stent implanted in the same session as the culprit, upper right image), 3) a stable atherosclerotic lesion without a stent (lower left image) and 4) a stent implanted at least 3 months before imaging (lower right image); green arrowheads flag the plaque/stent. (**L**) A schematic representation of the study's findings that translate the "inside-to-outside" signal from the human coronaries to their PVAT into an imaging application. P-values derived from unpaired t-test (A, F, H), one-way ANOVA (B-E), two-way ANOVA (G), or Wilcoxon signed rank test (J).

Supplementary Material

Imaging phenotyping of perivascular fat by computerised tomography detects human coronary inflammation

Authors: Alexios S. Antonopoulos[1]†, Fabio Sanna[1]†, Nikant Sabharwal[2], Sheena Thomas[1], Evangelos K Oikonomou[1], Laura Herdman[1], Marios Margaritis[1,3], Cheerag Shirodaria[2], Anna-Maria Kampoli[1], Ioannis Akoumianakis[1], Mario Petrou[4], Rana Sayeed[4], George Krasopoulos[4], Constantinos Psarros[1], Patricia Ciccone[1], Carl M. Brophy[1], Janet Digby[1], Andrew Kelion[2], Raman Uberoi[5], Suzan Anthony[5], Nikolaos Alexopoulos[6], Dimitris Tousoulis[6], Stephan Achenbach[7], Stefan Neubauer[1,3,8], Keith M Channon[1,3,8], Charalambos Antoniades[1,3,8]*

Affiliations:

[1]Division of Cardiovascular Medicine, Radcliffe Department of Medicine, University of Oxford,, UK

[2]Cardiothoracic Directorate, Oxford University Hospitals NHS Foundation Trust, Oxford, UK

[3]Oxford Centre of Research Excellence, British Heart Foundation, UK

[4]Department of Cardiothoracic Surgery, Oxford University Hospitals NHS Foundation Trust, Oxford, UK

[5]Department of Radiology, Oxford University Hospitals NHS Foundation Trust, Oxford, UK

[6]Athens University Medical School, 1st Department of Cardiology, Greece

[7]Medizinische Klinik 2, Universitätsklinikum Erlangen, Erlangen, Germany

[8]Oxford Biomedical Research Centre, National Institute of Health Research, UK

Supplementary Text

Detailed Material and Methods

Study design

Study Arm 1 comprised 453 patients undergoing coronary artery bypass grafting surgery (CABG) (Table S1). Exclusion criteria were any inflammatory, infectious, liver / renal disease or malignancy. Patients receiving non-steroidal anti-inflammatory drugs were also excluded. During surgery, adipose tissue samples were harvested: ScAT (from the site of the chest incision, n=374), ThAT (from the central thoracic area, attached to the pericardium, n=417) and EpAT (from the site of the right atrioventricular groove, away from any visible vessel, n=264). Samples were snap-frozen for gene expression studies, histology and CT imaging as explants, as described below. A subgroup of 105 patients also underwent CTA, as described below, the aim being to link the histological and biological characteristics of the adipose tissue biopsies, with the imaging characteristics of the same adipose tissue depots in vivo and in vitro.

Study Arm 2 comprised 45 patients undergoing CABG, with the same inclusion/exclusion criteria as Study Arm 1 (table S1). Paired samples of PVAT (adjacent to the proximal RCA) and non-PVAT EpAT (from an area 2 cm away from the RCA, over the right ventricle and not in close proximity with any other coronary arterial branch) were harvested for gene expression studies. In addition, samples of aortic tissue (collected as "buttons" from the site of the anastomosis of bypass grafts on the ascending aorta) were collected and used for *ex vivo* co-culture experiments with primary adipocytes as described later.

Study Arm 3 included a clinical cohort of 273 patients who underwent diagnostic coronary CTA (156 with and 117 without significant coronary artery disease, table S3). This cohort was

used to validate the findings generated from Study Arms 1 and 2 and translate them in a clinical setting.

Study Arm 4 included 19 patients with CAD (table S3): (a) 10 with an acute MI who had a CTA within 72h of their hospital admission, and after they had an invasive angiogram with a stent implantation at the site of the culprit lesion. Seven of these patients had stent implantation in a non-culprit lesion in the same session, and these lesions were used as controls (non-culprit lesions of unstable patients). The CTA was then repeated 5 weeks after the event (n=5). (b) 5 patients with stable coronary artery disease on optimum treatment, who underwent 2 CTAs with 5 weeks difference, and served as controls for the MI patients and (c) 11 patients with stable coronary artery disease under optimum treatment, who underwent stent implantation in a coronary artery at least 3 months before their CTA, and they were used as additional controls of the MI patients, to adjust for any possible artefact induced by the stent in the culprit lesions. This Study Arm was used to explore the capacity of FAI_{PVAT} to detect changes in PVAT in response to variations of vascular inflammation, i.e. to explore its ability to identify vulnerable atherosclerotic plaques and monitor the resolution of local vascular inflammation due to plaque rupture, during the post-MI period.

Histology studies

Adipose tissue sections, stored at -80° in optimal cutting temperature (OCT) media were cut into 15 micron sections and fixed onto slides. Non-specific antigen binding was blocked using serum-free protein block for 1-2h (#X0909, Dako). The staining was developed using the DAB Substrate kit for Peroxidase (#SK-4100, Vector Laboratories). The slides were mounted with Neo-Mount (#109016, Merck). Cell size was quantified under a bright field microscope. For each patient 3 different fields were quantified per depot using Image J software (V1.48).

Immunohistochemistry studies.

Adipose tissue sections were cryofrozen in OCT and cut into 5uM slices and fixed into slides using acetone fixation. Slides were then blocked for 1 hour at room temperature (RT) using Protein Block Serum-Free (Dako). Subsequently slides were incubated overnight at 4^{o}C with primary antibody [Anti-DLK (Abcam, ab21682), 1:250 dilution) anti-CD68 (DAKO, 1:1000 dilution), anti-CCR7 (Thermo scientific, PA5-24921, 1:25 dilution) and anti-CD206 (Mannose receptor, Abcam, ab64693 dilution 1:1000). Following the incubation slides were washed 3 times with PBS-T and incubated for 1 hour at RT with ImmPRESS HRP Anti-Rabbit IgG (Peroxidase) Polymer Detection Kit secondary antibody (Vector labs) and developed using DAB Peroxidase (HRP) Substrate Kit (Vector labs) and mounted using CC/Mount tissue mounting medium (Sigma). Pictures were taken using a Leica DM 2500 bright field microscope.

Gene expression studies

Samples of adipose (or adipocytes) and aortic tissue were snap frozen in QIAzol (Qiagen) and stored at -80^{o}C. RNA was extracted using the RNeasy Micro or Mini kit (Qiagen) and ribonucleic acid was converted into complementary DNA (Quantitect Rev. Transcription kit - Qiagen).The cDNA was then subjected to qPCR using TaqMan probes (Applied Biosystems) for *PPAR-γ* (Assay ID: Hs01115513_m1), *CEBPA* (Assay ID: Hs00269972_s1), *FABP4* (Assay ID: Hs00609791_m1), *CCR7* (Assay ID: Hs01013469_m1), *MRC1* (Assay ID: Hs00267207_m1), *CD68* (Assay ID Hs02836816_g1), *PREF1* (Assay ID: Hs00171584_m1), *TNFA* (Assay ID Hs01113624_g1), *IL6* (Assay ID Hs00985639_m1) and *IFNγ* (Assay ID Hs00989291_m1). Cyclophilin A (*PPIA*) was used as house-keeping gene for the adipose tissue and adipocytes

(Assay ID Hs04194521_s1) and *GAPDH* for the aortic tissue (Assay ID Hs02758991_g1). The reactions were performed in triplicate in 384-well plates, using 5 ng of cDNA per reaction, on an ABI 7900HT Fast Real-Time PCR System (Applied Biosystems). The efficiency of the reaction in each plate was determined based on the slope of the standard curve; expression of each gene of interest relative to its housekeeping gene was calculated using the Pfaffl method.

Aortic tissue/adipocyte co-cultures

To test whether the arterial wall of patients with advanced atherosclerosis generates inflammatory mediators able to prevent the preadipocyte lipid accumulation in PVAT in a paracrine way, aortic tissue was harvested from patients undergoing CABG, and co-cultured with preadipocytes isolated from PVAT surrounding the RCA of the same patients. The aortic samples were processed using the tissue explant method, in the presence/absence of angiotensin II 100 nM for a week to induce additional vascular inflammation. At the same time, preadipocytes were isolated from the PVAT attached to the RCA of these patients, by digesting the PVAT for 45 minutes at 37^{o}C in a solution of collagenase H (1 mg/mL in PBS). The digested tissue was then centrifuged at 1200 rpm for 5 minutes and re-suspended in DMEM/F-12 supplemented with 10% FBS and 0.25ng/mL human FGF. Preadipocytes and aortic tissue (±angiotensin II) were cultured for 1 week separately. At the end of the week, the aortic tissue was washed to remove angiotensin II and co-cultured with the isolated primary preadipocytes. When the preadipocytes were confluent around the aortic tissue, they were differentiated in differentiation medium; DMEM/F12 supplemented with 0.5 mM 3-isobutyl-1-methylxanthine (IBMX), 100 nM insulin, 100nM dexamethasone, 2 nM triiodo-L-thyronine (T3), 10 μg/ml transferrin, 1μM rosiglitazone, 33 μM biotin and 17 μM pantothenic acid, 3% FBS for 7 days followed by adipocytes maintaining media containing DMEM/F12 with 10nM

insulin, 10nM dexamethasone for 2 days. Adipocytes were monitored for cell size and lipid accumulation visually and by staining with oil-red O followed by quantification using Image J (version 1.48) at day 9. In parallel experiments, expression of inflammatory cytokines *IL-6+TNF-α+IFN-γ* in aortic tissue biopsies was measured using RTPCR, after 7 days culture ±angiotensin II 100 nM.

Adipocyte cultures

The effect of inflammatory cytokines, TNF-α (4 ng/ml)+IL-6 (25 ng/ml)+IFN-γ (20 ng/ml), on perivascular adipocyte differentiation and lipid accumulation was tested by incubating primary preadipocytes isolated from PVAT of patients undergoing CABG. Preadipocytes were exposed to differentiation media for 7 days followed by incubation in adipocyte maintaining media for 2 days. Images were taken every 3 days during differentiation and RNA was isolated at each time point. The degree of differentiation of the preadipocytes was estimated by a) the changes in adipocyte morphology and size b) the accumulation of lipid droplets (stained using oil-red-o) c) the increased expression of adipocyte differentiation markers, *PPAR-γ, CEBPA* and *FABP4* d) the reduced expression of *Pref-1*.

Adipocyte proliferation assay

Human preadipocytes isolated from PVAT (peri-coronary AT) were cultured in 96 well plates (5×10^3 cells per well) for 24h. Then paired wells were treated with/without TNF-α (4 ng/ml)+IL-6 (25 ng/ml)+IFN-γ (20ng/ml) for 24h and 48h. A 20μL CellTiter 96 AQueous One Solution Reagent (Promega) was added to each well and the plates were incubated for 2 h at 37 °C. Subsequently, absorbance at 490 nm was measured using a 96-well plate reader.

Oil-red O staining

At day 9 of the differentiation time course, adipocytes were washed twice with PBS and fixed with paraformaldehyde 4% for 10 minutes at room temperature. Cells were rinsed with distilled water followed by a 5 minutes wash with 60% isopropanol. Cells then were stained for 10 minutes with a solution of oil-red O (0.3g oil-red O, Sigma Aldrich) in 100 mL of isopropanol diluted in water) and finally washed with tap water. Nuclei were counterstained with a solution of hematoxylin. Formation of lipid droplets was observed by phase contrast microscopy. To quantify the amount of lipid droplets accumulated in mature adipocytes, cells stained with oil-red O were washed with a solution of 60% isopropanol in order to extract the oil-red O. The absorbance of the dye was quantified by spectrophotometer, at 500 nm. For the co-culture experiments of adipocytes with aortic tissue, quantification of oil-red-O was performed using image analysis of the fixed slides using Image J (version 1.48). This was to avoid the quantification bias derived from the fact that adipocytes do not grow under the aortic tissue samples, leading to a variable surface area of growing adipocytes per well.

Computerised tomography studies

Participants in Study Arms 1 and 3 underwent CTA using a 64-slice scanner (LightSpeed Ultra, General Electric). Heart rate was optimised using intravenous injection of beta-blockers and sublingual glyceryl-trinitrate (800ug) was also administered to achieve maximum coronary vasodilatation. A non-contrast prospectively ECG triggered axial acquisition CT scan was obtained (0.35 sec rotation time, 2.5 mm axial slice thickness, 20mm detector coverage, tube energy of 120 kV and 200 mA) with the carina and the diaphragm used as cranial and caudal

landmarks respectively. Lung field of view was extended to cover the entire thoracic soft tissue (for ScAT analysis). CTA was performed following intravenous injection of 95ml of iodine based contrast medium (Niopam 370, BRACCO) at a flow rate rate of 6mL/sec (tube energy of 120 kVp, axial slice thickness of 0.625 mm, rotation time of 0.35 sec, detector coverage of 40 mm). Prospective image acquisition was used by ECG-gating at 75% of cardiac cycle (with 100 msec padding for optimal imaging of the right coronary artery if required). Participants with step artefacts on acquisition or sub-optimal RCA imaging were excluded from any further analyses (in total 6 participants or 1.6% of the patients undergoing CTA).

Adipose tissue characterization by CT: The reconstructed images were transferred to an offline image processing and analysis workstation (Aquarius Workstation V.4.4.11 TeraRecon). Adipose tissue was defined as all voxels with attenuation between -190 and -30 Hounsfield Units (HU). Voxel attenuation histograms were plotted and the Fat Attenuation Index (FAI) was defined as the average CT attenuation of the adipose tissue volume of interest (within the pre-specified window of -190 to -30 HU). The working hypothesis was that adipocyte lipid content is the main driver of FAI; since larger adipocytes have a higher proportion of lipid phase (adipocytes) compared to aqueous phase (extracellular space), this would lead to more negative FAI. EpAT was tracked by contouring of the pericardial sac in a semi-automated method (starting from the bifurcation of the pulmonary artery at the most cranial point up to the apex of the heart at the most caudal point). Intrathoracic adipose tissue (ThAT) included all intrathoracic fat located between the pulmonary artery bifurcation and the diaphragm, and was estimated as a surrogate marker of obesity. ScAT was tracked by sampling of all thoracic subcutaneous AT, at the height of the caudal end of sternum and extending cranially for a total of 25 mm. FAI was calculated in EpAT (FAI_{EpAT}) and ScAT (FAI_{ScAT}) from the 3D reconstructed images using a research version of Aquarius Software

(V.4.4.11, Terarecon), developed in the context of the current research programme. Patient scans in Study Arm 1 were performed both with and without a contrast agent, to assess the impact of the contrast agent on the absolute values of FAI measured.

Peri-coronary adipose tissue characterization: 3D curved multiplanar reconstruction was used to define the vascular segment of interest and to analyse perivascular tissue. The right coronary artery (RCA) was used to perform pericoronary adipose tissue imaging, since this coronary artery has no major branches and PVAT / non-PVAT can be easily defined. The first 1cm of the proximal RCA was omitted to exclude adipose tissue lying close to the coronary ostium/aortic root from the analysis. A 4 cm-long segment of the RCA (10^{th} to 50^{th} mm from the RCA ostium) was tracked in an automated way. Inner and outer layers of analysis were manually optimised to track lumen and outer wall boundaries respectively. Perivascular tissue was then segmented in a semi-automated way into 20 concentric cylindrical 1mm-thick layers around the outer vascular wall. FAI was calculated for each layer of tissue. The FAI curves of adipose tissue were plotted against the radial distance from the outer vascular wall.

FAI of PVAT (FAI_{PVAT}): There is no clear biological definition of PVAT. Therefore we defined FAI_{PVAT} as the FAI of adipose tissue in a layer of tissue within a radial distance from outer coronary artery wall equal to the average diameter of the tracked RCA segment. Non-PVAT FAI ($FAI_{non-PVAT}$) was defined at the most distal concentric layer of adipose tissue from RCA wall. Volumetric Perivascular Characterisation Index (VPCI) was then calculated as the %change in FAI from PVAT (FAI_{PVAT}) to non-PVAT (2cm away from the RCA's outer wall, $FAI_{non-PVAT}$), as defined above ($VPCI=[100x(FAI_{PVAT}–FAI_{non-PVAT})/|FAI_{PVAT}|]$). The method of FAI_{PVAT} calculation had excellent intra and inter-observer reproducibility (0.22% and 0.53% respectively). PVAT volume

was also calculated around the same 40-mm segment of the RCA within a constant-volume layer of tissue surrounding the RCA.

Coronary calcium score: Coronary calcium score (CCS) was measured on Aquarius Workstation® for all coronary arteries (RCA quantified separately), by calculating the Agatston score.

Coronary plaque analysis using CTA: For analysis of vascular plaque morphology, HU mapping of the RCA wall was used to quantify fibrous plaque (65 to 265 HU) and calcification volume (>465 HU). Atherosclerotic plaque burden was calculated as the ratio of fibrous plaque volume to total vessel volume. Low atherosclerotic plaque burden in RCA was defined as atherosclerotic plaque burden in the lowest tertile.

Analysis of FAI_{PVAT} in Study Arm 4: CTA was performed in MI patients after coronary stent implantation (within 72h). A similar (control) population of patients who underwent coronary stent implantation at least 3 months before CTA was also included, to account for possible artefacts from the stent. Stented coronary vessels were divided into 3 segments and FAI_{PVAT} was calculated for the PVAT surrounding each vascular segment (proximal, middle and distal segment), while the analysis of FAI_{PVAT} was extended proximally and distally of the stented area as indicated. For the patients that underwent a second scan at 5 weeks, the identical same segments of PVAT were analysed, as in the baseline CTA on a Toshiba Aquilion CX 128-slice CT scanner.

CT scans of adipose tissue explants

Frozen explants of ScAT, ThAT and EpAT from patients in Study Arm 1 were scanned, to evaluate the ability of FAI to describe adipocyte size. Adipose tissue explants were scanned on a Toshiba

Aquilion One 320-slice CT scanner, using dual energy helical acquisition with 135 keV and 80 keV, 50 mA, 0.5 sec rotation time, 0.5mm slice thickness, and image reconstruction at 120 keV for the FAI analysis. A subgroup of 105 patients from Study Arm 1 also had a CT scan, and the scans were used to validate the in vitro CT imaging model against in vivo imaging, allowing the use of this model to understand the biological value of FAI in the study of human AT.

Positron emission tomography/Computerised tomography imaging studies

To explore the ability of FAI to detect adipose tissue inflammation, we validated it against ^{18F}FDG uptake using PET/CT (which is the gold standard modality to assess tissue inflammation *in vivo*); for this purpose we analysed simultaneously FAI_{ScAT} and ^{18F}FDG uptake in paired PET and CT images from 40 subjects (25 males/15 females) who had an ^{18F}FDG PET/CT scan performed under a clinical indication.

PET/CT examinations were performed on a 3D mode time of flight (ToF) GE Discovery 690 PET/CT system (GE Healthcare). The patients fasted for at least 6 h prior to their scan. Their blood glucose was measured prior to intravenous injection, with 4 MBq/kg of ^{18F}FDG. Imaging commenced 90 min post-injection (93±7 min) and covered the skull base to upper thighs. The PET/CT images were acquired under normal tidal respiration for 4 min per bed position. The CT was performed using a pitch of 0.984, 120 kV, auto mA with a noise index of 25. PET images were reconstructed using two different algorithms both of which used the CT for attenuation correction and the same normalisation correction factors. The standard of care PET reconstruction algorithm used is ToF OSEM (VPFX, GE Healthcare). This was used with two iterations, 24 subsets and 6.4 mm Gaussian filter in our institution. The sinograms generated at the time of

scanning were retrospectively processed using the new ToF BPL reconstruction algorithm (Q.Clear, GE Healthcare).

Acquired PET and CT images were then analyzed using the Terarecon Aquarius iNtuition V.4.4.11 software. The analysis of the ScAT was performed on axial images at the caudal end of the sternum. Circular regions of interest (ROI) were drawn at the midline anteriorly to the sternum on three consecutive slices. The diameter of all three ROIs was equal to the visible depth of the ScAT depot and was consistent between slices in the same patient. Mean SUV and FAI for each ROI were automatically calculated by the software and then averaged to calculate overall mean SUV and FAI for all tracked ScAT in each patient. To calculate the target-to-background ratio (TBR), 3 circular ROIs each with a diameter equal to 15mm were drawn in the lumen of the pulmonary artery at the level of the pulmonary artery bifurcation on three consecutive slices and the average of the mean SUV values of all three ROIs was calculated. TBR for ScAT was then calculated by dividing target (ScAT) mean SUV by background (PA lumen) mean SUV.

For EpAT, a similar methodology was used, by tracking 3 polygonal ROI on consecutive axial slices along the upper third of the right atrioventricular groove (where epicardial fat is most abundant); mean SUV and FAI for tracked EpAT were determined and then TBR was calculated by dividing target (EpAT) mean SUV by pulmonary artery lumen mean SUV. Nevertheless assessment of EpAT inflammation by ^{18F}FDG PET /CT had limitations due to increased background noise from the adjacent myocardium (fig S9, which has significantly higher metabolic activity compared to adipose tissue and highly increased radiotracer uptake, resulting in an intra- and inter-observer CV for TBRmean of EpAT of 11.76% and 14.36% respectively) and therefore we chose to limit our analysis only to isolated adipose tissue depots, such as ScAT.

Definition of high vs low adipose tissue inflammation based on ^{18F}FDG uptake. In order to define high versus low adipose tissue inflammation, TBR values were set at 0.173 (33rd percentile), 0.20 (50th percentile) and 0.23 (67th percentile); for a cut-off value of 0.20, area under the curve (AUC) was 0.971 (95% confidence intervals 0.924-1.000, p<0.0001). After setting a FAI cut-off value of -113.3, sensitivity and specificity for prediction of high adipose tissue inflammation were 90% and 100% respectively. For a TBR cut-off of 0.173, AUC was 0.791 (95% CI 0.646-0.937, p=0.0033) with FAI values greater (less negative) than -113.3 predicting high adipose tissue inflammation with a sensitivity of 73% and a specificity of 100%. Finally, setting the TBR cut-off at 0.237 resulted in an AUC of 0.894 (95% CI 0.791-0.996, p<0.0001) with FAI values greater than -113.3 identifying highly inflamed adipose tissue with a sensitivity of 100% and specificity of 81%

Technical considerations: Given that coronary CTA is routinely performed using an ionic contrast agent, we also explored the possible confounding effect of the contrast agent on the calculated FAI in epicardial adipose tissue *in vivo* (fig S9). We found a strong linear association between the FAI of EpAT obtained from images with and without contrast agent administration (fig. S12). Due to the high regional histological heterogeneity of ThAT a meaningful matching of *in vivo* CT images with the biological characteristics of the respective tissue biopsies was not possible.

To assess the potential confounding effect of the contrast agent on the measured FAI_{PVAT} or VPCI, we used a subgroup of patients from Study Arm 3 (n=30) with no evidence of coronary atherosclerosis or coronary calcification (to avoid the bias from existing vascular disease) and explored the impact of the variation in contrast attenuation/volume in the RCA lumen on the measured FAI_{PVAT} around the proximal RCA (10 to 50mm from RCA ostial origin) and the respective VPCI. We observed no association between the average attenuation or the volume of

the luminal contrast with FAI_{PVAT} or VPCI (fig. S11). These data, in combination with the very weak association between the calcium in the underlying coronary artery and FAI_{PVAT} or VPCI, confirm that these novel indices are not driven by possible artefacts caused either by calcium deposition or the administration of contrast agent.

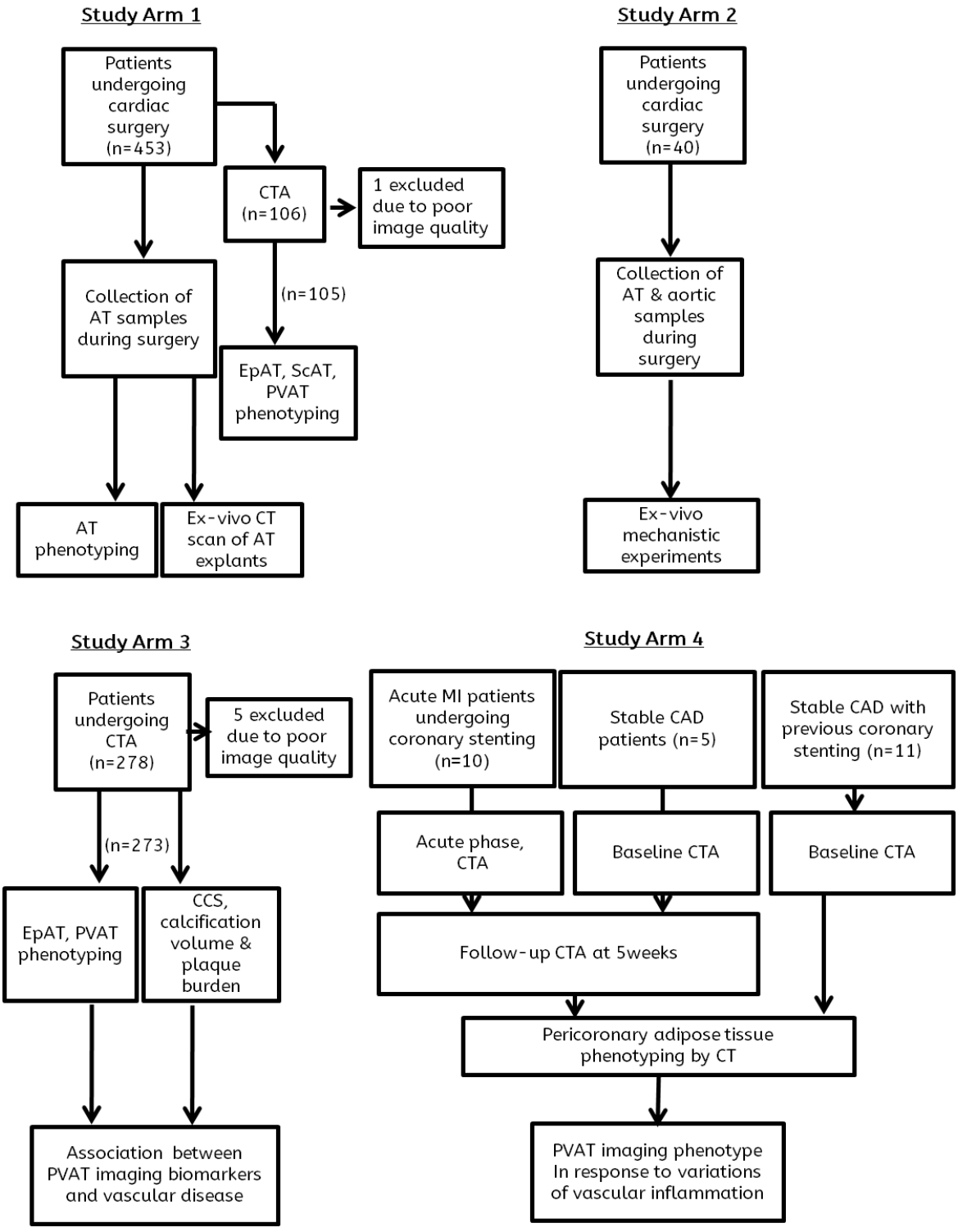

fig. S1. Study flow chart. MI: myocardial infarction; AT: adipose tissue; CAD: coronary artery disease; CCS: coronary calcium scoring: CTA: coronary computerised tomography angiography; EpAT: epicardial adipose tissue; PVAT: perivascular adipose tissue, ScAT: subcutaneous adipose tissue

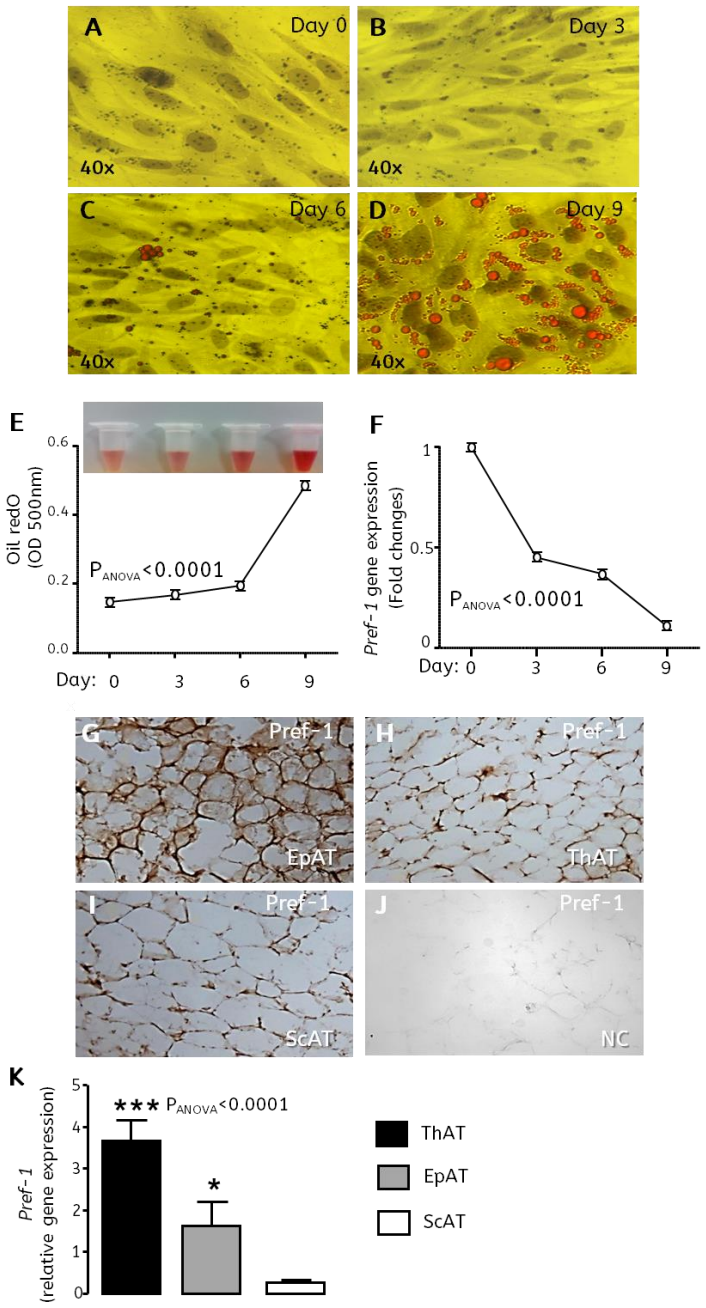

fig. S2. Adipocyte differentiation in-vitro and lipid accumulation. (**A-E**). Expression of Pref-1 (preadipocyte marker) from day 0 to day 9 (**F,** n=5). Immunohistochemistry for Pref-1 in subcutaneous (ScAT), thoracic (ThAT) and epicardial (EpAT) adipose tissue (**G-J**). Pref-1 expression data available in n=439 patients of Study Arm 1 (**K**). *P<0.05; *P<0.001 vs ScAT. NC: negative control. For E, F, & K: p-values from one-way ANOVA.

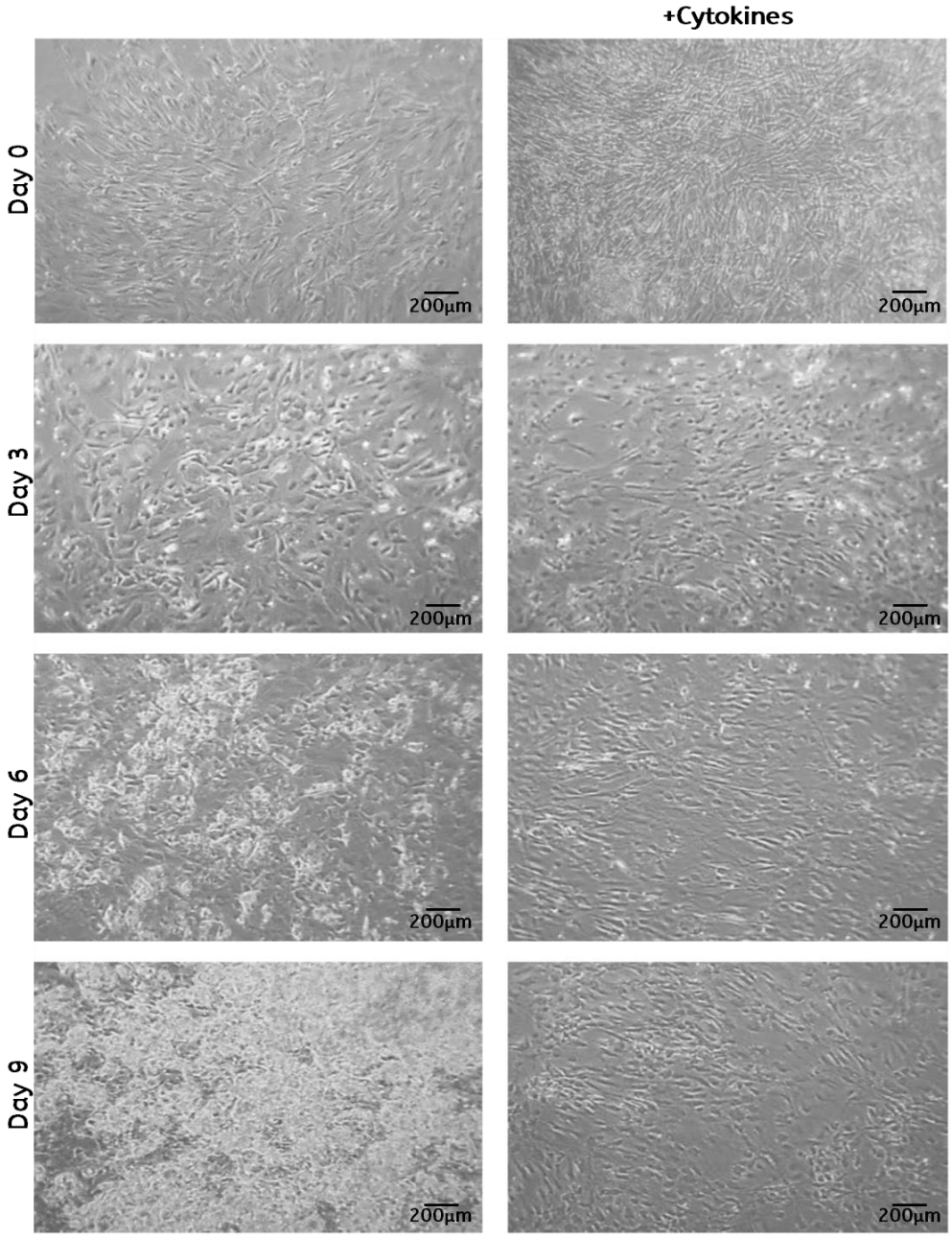

fig. S3. Effects of pro-inflammatory cytokines on pre-adipocyte differentiation. Human pre-adipocytes were isolated from peri-coronary adipose tissue harvested from patients undergoing coronary artery bypass grafting surgery, and differentiated to adipocytes in the presence or absence of proinflammatory cytokines (interleukin-6 25ng/mL + tumor necrosis factor-alpha 4ng/mL + interferon-γ 20ng/mL). Images from bright field microscope.

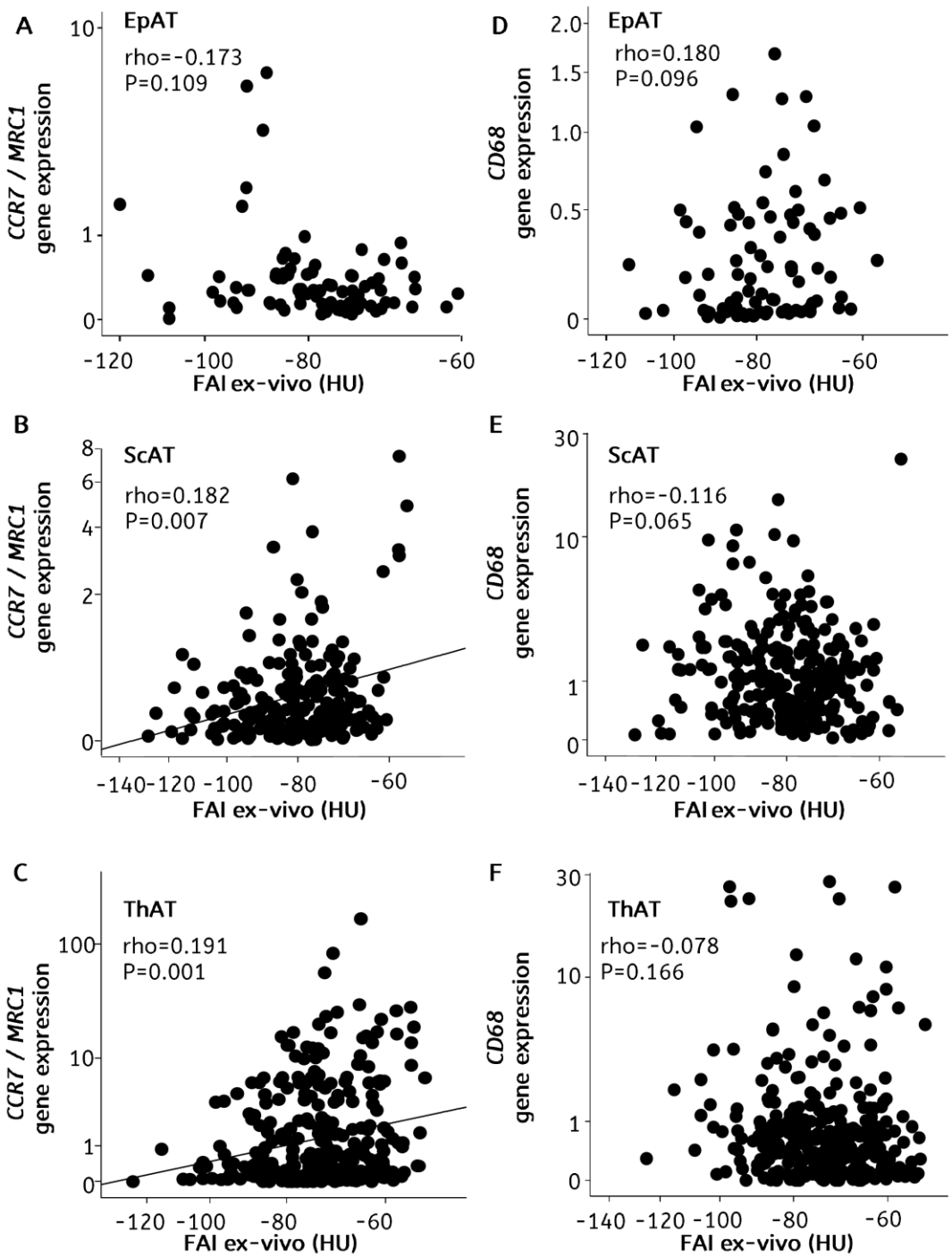

fig. S4. Fat Attenuation Index (FAI) and macrophage infiltration / macrophage polarization status in adipose tissue explants. Correlation between FAI of ex-vivo scanned adipose tissue explants and *CCR7/MRC1* (marker of M1/M2 polarisation status, **A-C**) and *CD68* (marker of macrophage infiltration, **D-F**) gene expression in the same tissue. EpAT: epicardial adipose tissue; ScAT: subcutaneous adipose tissue, ThAT: mesothoracic adipose tissue.

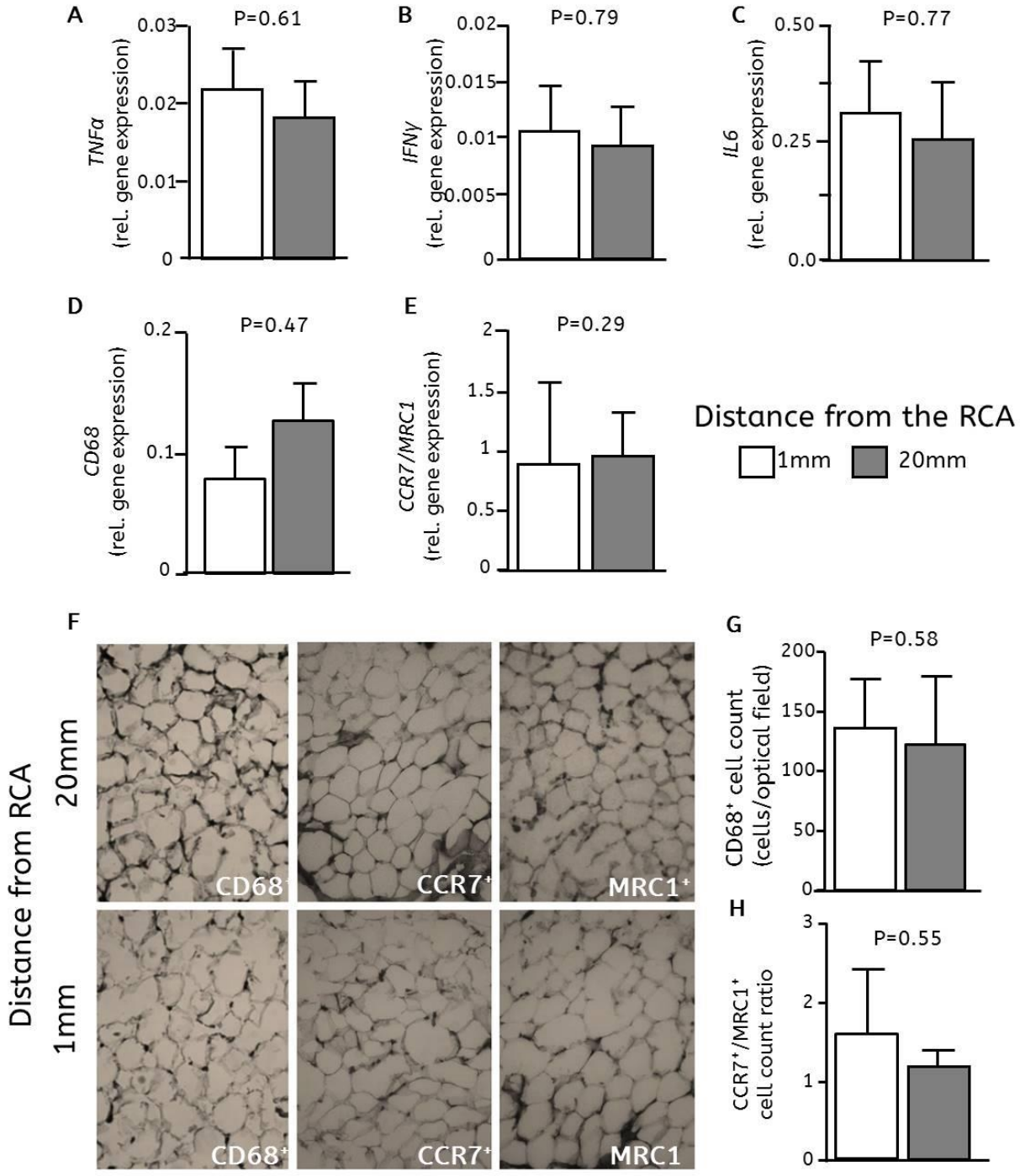

fig. S5. Gene expression of inflammatory cytokines and markers of macrophage infiltration/ polarization in coronary perivascular vs non-perivascular adipose tissue. Interleukin-6 (*IL-6*, **A**), tumor necrosis factor-α (*TNF-α*, **B**), interferon-γ (*IFN-γ*, **C**), *CD68* (**D**) and *CCR7/MRC1* (**E**) gene expression in perivascular adipose tissue (PVAT) and non-PVAT, around the right coronary artery (RCA, n=7-10). Representative immunohistochemistry images (**F**) and cell count (**G, H**, n=5-6) after staining for $CD68^+$, $CCR7^+$ and $MRC1^+$. P-values from Wilcoxon signed rank test.

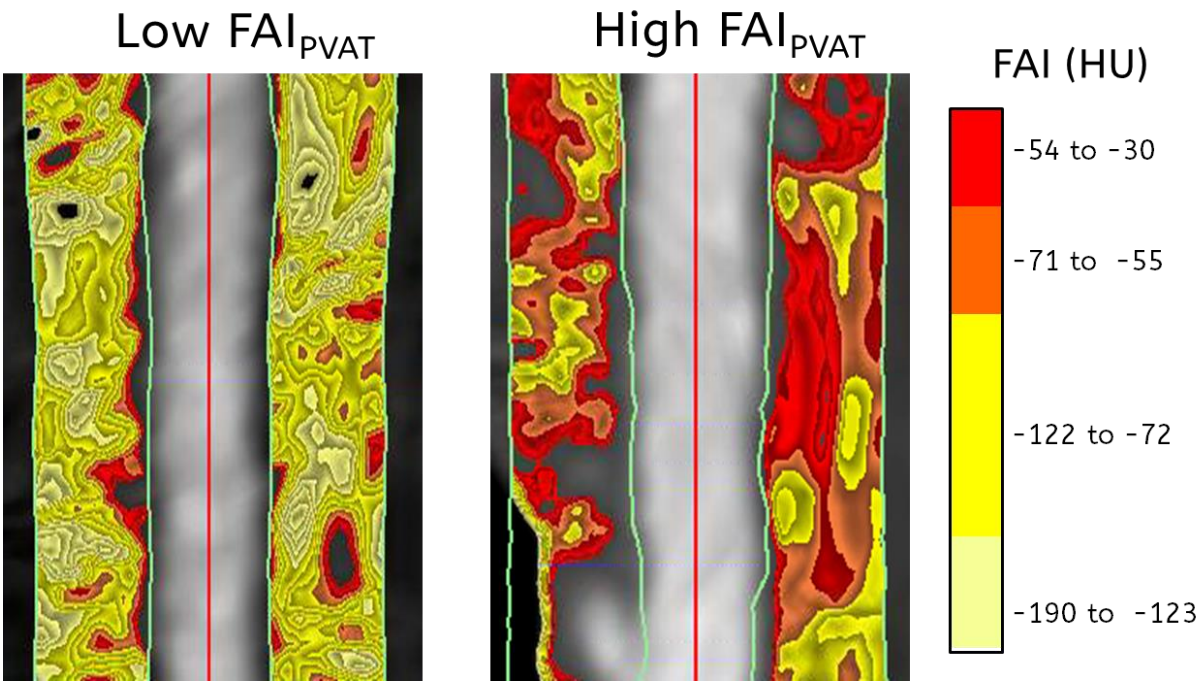

fig. S6. Variation in Fat Attenuation Index (FAI) mapping of pericoronary adipose tissue in the absence of vascular disease. Representative examples of two coronary arteries without significant plaque burden that have completely different fat attenuation index (FAI) colour mapping of the surrounding perivascular adipose tissue (PVAT).

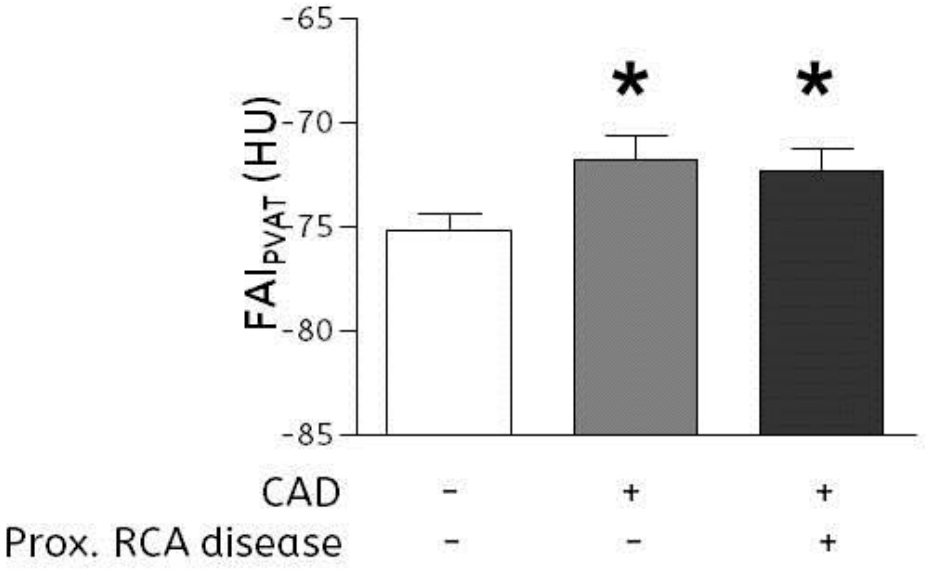

fig. S7. Perivascular adipose tissue Fat Attenuation Index (FAI_{PVAT}) and coronary artery disease (CAD). In 226 patients of study arm 3, patients with CAD were divided into two subgroups based on the existence of obstructive coronary disease (>50% stenosis of lumen diameter) in the proximal segment of the right coronary artery (RCA), which was used for calculation of FAI_{PVAT}. *P<0.05 vs no CAD/no prox RCA disease, calculated using unpaired t-test.

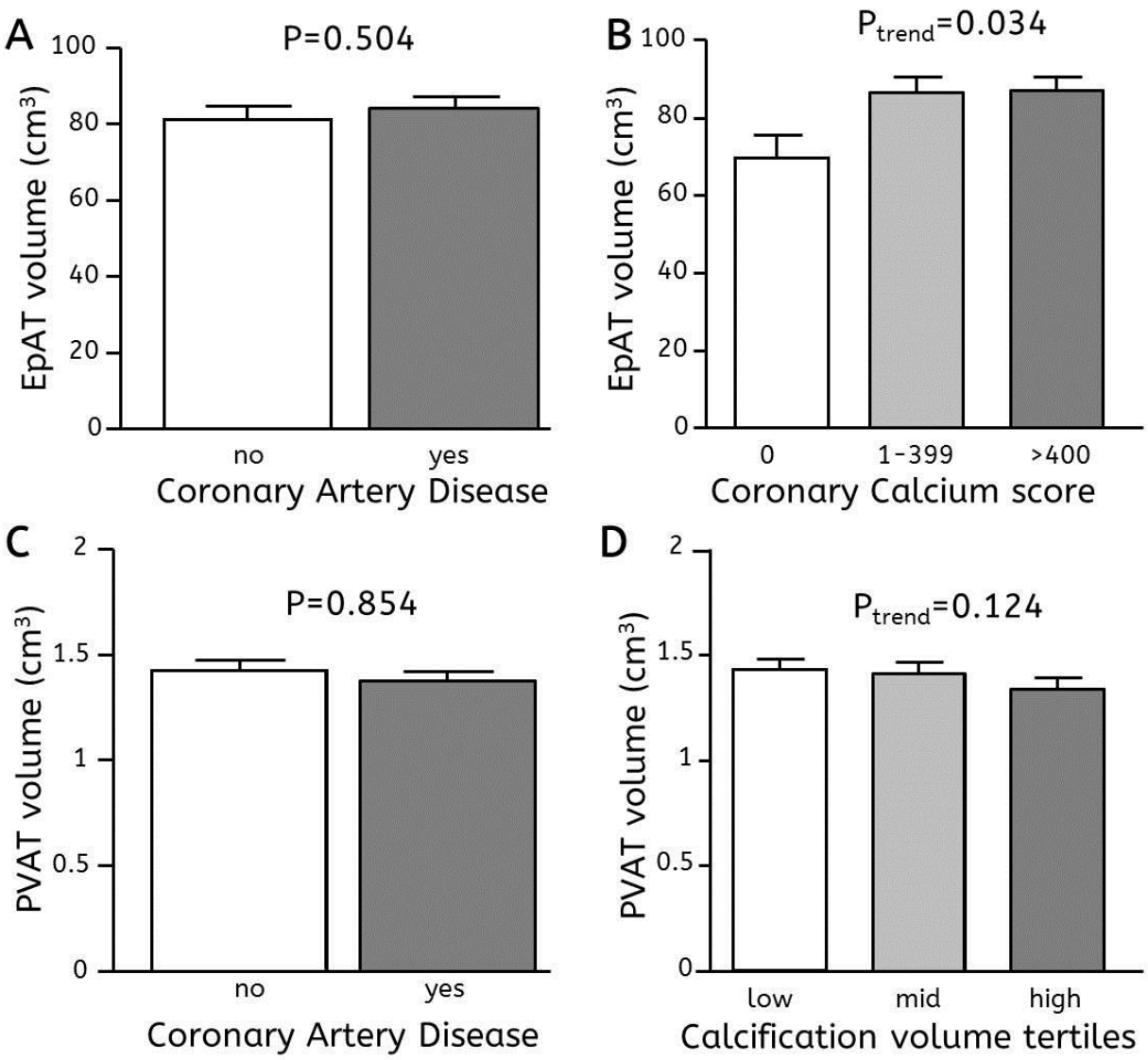

fig. S8. Associations between epicardial and perivascular adipose tissue volumes and coronary atherosclerosis/calcification. Associations between epicardial adipose tissue (EpAT) volume and coronary artery disease (**A**) or coronary calcium score (**B**) in n=267 patients of Study Arm 3. Associations between perivascular adipose tissue (PVAT) volume and the presence of CAD (**C**) or the calcification volume in the underlying artery (**D**) in the same patients. p-values from unpaired t-test (A, C) or one-way ANOVA (B, D).

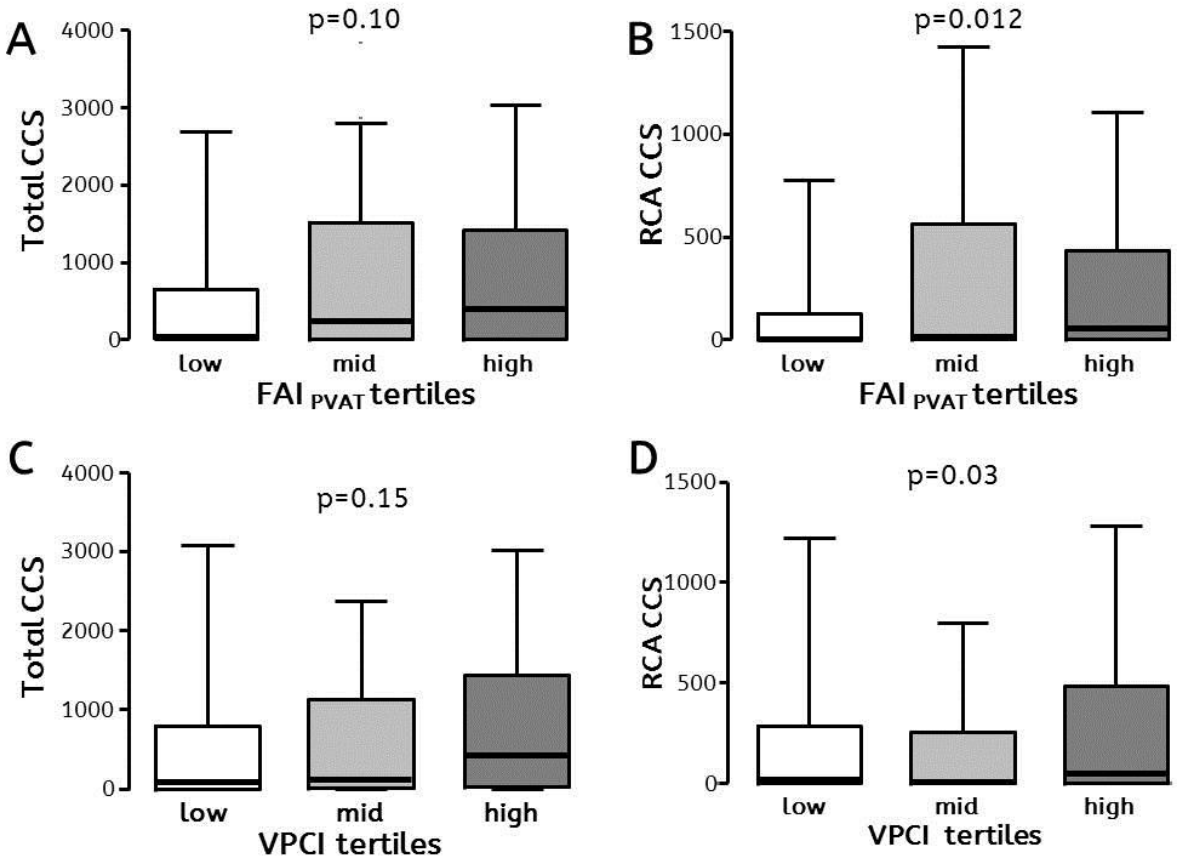

fig. S9. Associations between coronary perivascular adipose tissue imaging phenotyping and coronary and coronary calcium score. Associations between Fat Attenuation Index of perivascular adipose tissue (FAI_{PVAT}) around the proximal right coronary artery (RCA) and total coronary calcium score (CCS, **A**) or RCA CCS (**B**) in 255 patients of Study Arm 3. Associations between Volumetric Perivascular Characterization Index (VPCI) of the same RCA segment and total CCS (**C**) or RCA CCS (**D**).

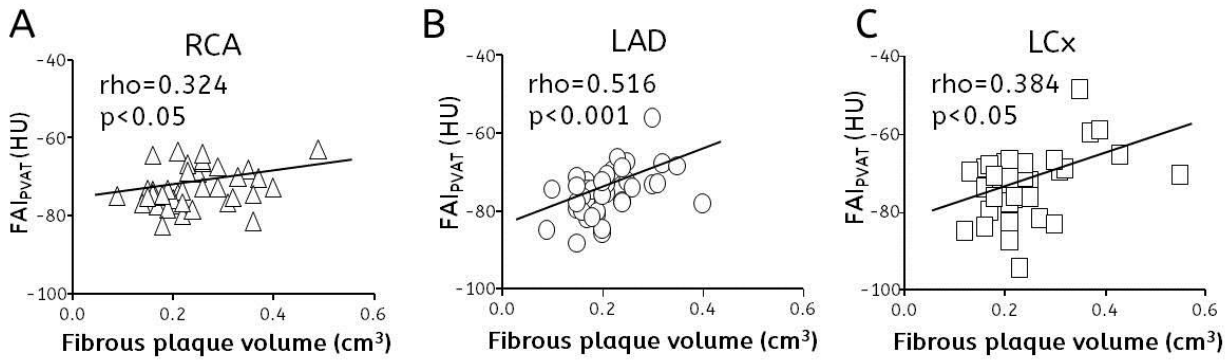

fig. S10. Correlations between perivascular adipose tissue Fat Attenuation Index (FAI_{PVAT}) and coronary plaque burden in major epicardial arteries. In a subgroup of 40 patients from Study Arm 3 FAI_{PVAT} was analysed around a 40mm proximal segment of all three major epicardial coronary arteries (10mm away from their ostium) to demonstrate the technical feasibility of the method. Correlations between FAI_{PVAT} and fibrous plaque volume in the underlying coronary segment of left anterior descending (LAD, **A**), left circumflex (LCx, **B**) and right coronary artery (RCA, **C**)

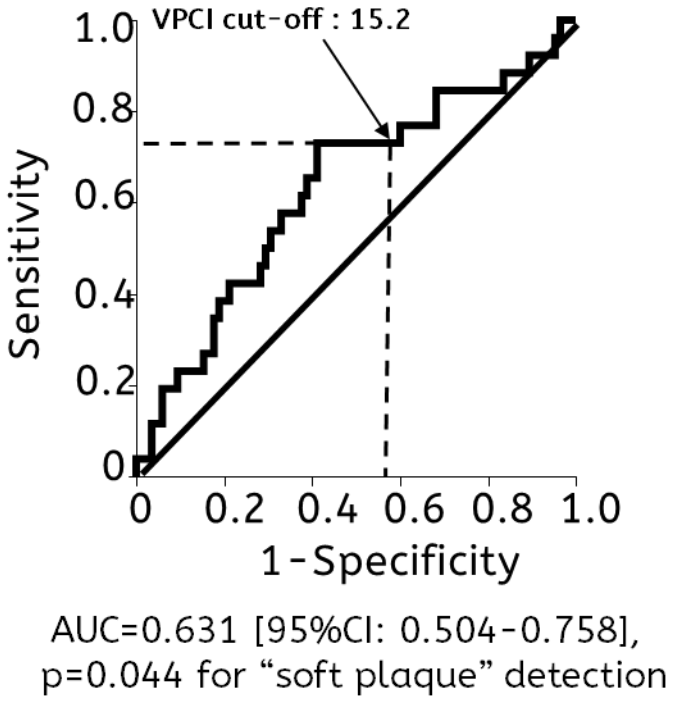

fig. S11. Detection of non-calcified plaques in human coronaries by CT imaging mapping of pericoronary adipose tissue. Receiver Operating Characteristics (ROC) curve analysis for the ability of VPCI to detect the presence of soft (non-calcified) atherosclerotic plaques in the RCA (within the top 2 tertiles). A cut-off value of VPCI equal to the median (15.2) was diagnostic for presence of non-calcified plaques with a sensitivity of 73.1% and specificity of 58.8%, as demonstrated (n=110).

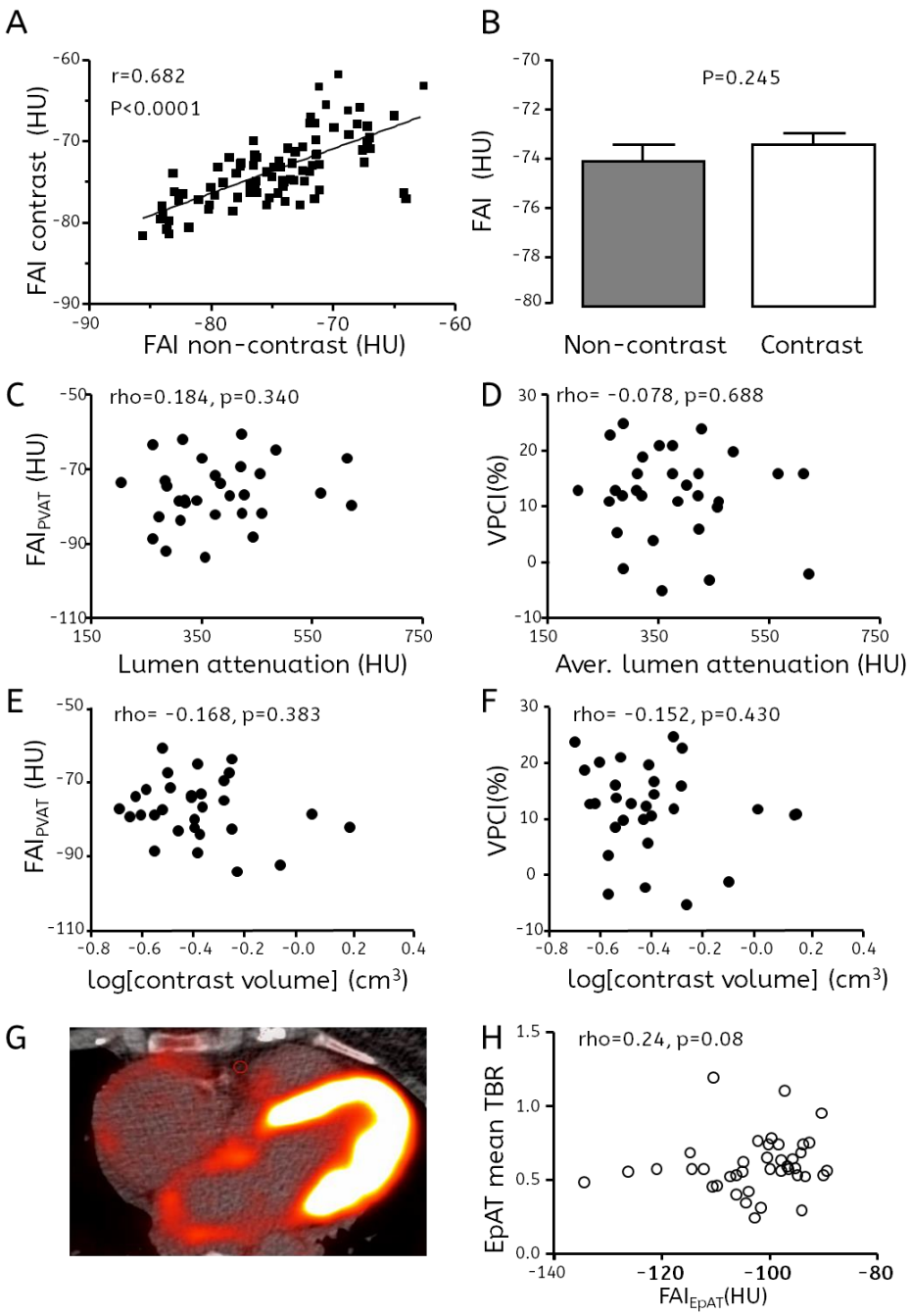

fig. S12. Technical considerations related to calculation of Fat Attenuation Index (FAI). Correlation between FAI_{EpAT} in paired contrast and non-contrast images (**A)** and comparison of the respective absolute values **(B)**. Associations between lumen attenuation and Fat Attenuation Index for perivascular adipose tissue (FAI_{PVAT}, **C**) and Volumetric Perivascular Characterisation Index (VPCI, **D**) in a pilot subgroup of 30 healthy individuals from Study Arm 3 (without detectable plaque or calcium in proximal right coronary artery). Associations between contrast volume in coronary lumen and FAI_{PVAT} (**E**) or VPCI (**F**). ^{18}F-FDG uptake by EpAT in PET/CT studies demonstrating increased background noise and ^{18}F-FDG "spill over" from the adjacent myocardium (**G**). Association between EpAT mean Target-to-background ratio (TBR) and FAI_{EpAT} (**H**). p-values in B from paired t-test.

Table S1. Demographic characteristics of study participants

	Study arm 1		**Study arm 2 (ex vivo studies)**
	All (CT adipose tissue explants)	***CTA (in vivo)***	
Participants (n)	453	105	45
Age (years)	66.8±0.49	65.0±0.97	65.9±1.39
Male gender (%)	80.8	86.9	80
Hypertension (%)	70.9	74.8	84.4
Hyperlipidaemia (%)	75.5	88.8	88.9
Type 2 diabetes (%)	24.1	28.2	13.3
Smoking (ex/active) (%)	53.0/11.3	51.4/12.1	55.6/6.7
BMI (Kg/m^2)	28.4±0.2	28.7±0.4	28.8±0.6
Cholesterol (mg/dl)	4.35±0.18	5.20±0.50	5.1±0.31
HDL (mg/dl)	1.19±0.06	1.08±0.06	1.43±0.07
Glucose (mg/dl)	111.8±2.16	113.9±4.6	109.5±7.8
Insulin (μU/ml)	11.0±1.5	11.5±2.9	8.1±1.2
HOMA-IR*	1.40 [0.81-2.50]	1.66 [0.97-2.52]	2.32±0.52
Medication (%)			
ACEi	48.5	45.8	42.2
ARBs	14.3	17.8	15.6
Beta blockers	64.8	74.8	66.7
Aspirin/Clopidogrel	79.2/24.0	86.0/37.4	73.3/26.7
Statins	80.8	86.9	80.0
CCBs	26.8	31.8	22.2

ACEi: Angiotensin converting enzyme inhibitors; ARBs: Angiotensin receptor blockers; BMI: Body mass index; CAD: Coronary artery disease; CCBs: Calcium channel blockers; CCTA: Coronary Computerised tomography angiography; HOMA-IR: Homeostatic model of insulin resistance; HDL: High density lipoprotein; ThAT vol: intrathoracic adipose tissue volume. Continuous variables expressed as means+/-SEM or *median[25^{th}-75^{th} percentile].

Table S2. Range of FAI values in adipose tissue explants and *in vivo*

	FAI range (HU)		
	Low tertile	***Mid tertile***	***High tertile***
Scans of AT explants (see Fig. 4)			
Epicardial AT	-120 to -84.3	-84.1 to -73.0	-72.9 to -52.7
Thoracic AT	-125 to -77.7	-77.6 to -68.7	-68.6 to -49.8
Subcutaneous AT	-128.0 to -84.4	:-84.3 to -74.2	-74.1 to -56.1
Scans of AT *in vivo* (see Fig. 5)			
Epicardial AT	-81.6 to -74.7	-74.8 to -70.7	-70.9 to -61.0
Subcutaneous AT	-108.0 to -101.0	-101.0 to -97.0	-97.0 to -89.0

Scans of adipose tissue (AT) explants correspond to the data presented in Fig.4, performed in tissue from 453 patients undergoing cardiac surgery, while scans of AT in vivo correspond to the data presented in Fig. 5, performed in a subgroup of 105 patients undergoing cardiac surgery.
FAI: Fat Attenuation Index

Table S3. Demographic characteristics of study participants in study arms 3 & 4

	Study arm 3		**Study arm 4**		
	No CAD	***CAD***	***MI***	***Stable CAD***	***Stable CAD - stent***
Participants (n)	117	156	10	5	11
Age (years)	58.6±1.0	64.5±0.8*	53.2±3.4	63.2±2.1	58.8±3.1
Male gender (%)	51.3	8.3*	80	80	63.6
Hypertension (%)	33.0	71.1*	10	80	72.7
Hyperlipidaemia (%)	25.5	78.2*	30	60	72.7
T2Ds (%)	8.5	29.4*	20	80	27.3
Smoking (ex/active) (%)	21.6/1.9	42.3/9.9*	20/40	40/20	9.1/18.2
BMI (Kg/m^2)	29.5±2.3	28.7±0.5	27.4±1.3	28.1±0.3	30.8±2.1
ThAT vol (cm^3)	216.1±11.4	263.9±22.2*	193.8±25.4	193.3±21.9	233.1±46.1
Medication (%)					
ACEi	5.1	37.8*	50	40	54.5
ARBs	3.4	14.7*	10	40	27.3
Beta blockers	16.2	62.2*	100	100	100
ASA/Clopidogrel	16.7/0	78.4/26.3*	100/60	100/40	90.9/36.4
Statins	17.9	77.7*	90	80	90.9
CCBs	7.7	24.4*	0	0	18.2

ACEi: Angiotensin converting enzyme inhibitors; AMI: acute myocardial infarction; ARBs: Angiotensin receptor blockers; ASA: acetylsalicylic acid; BMI: Body mass index; CAD: Coronary artery disease; CCBs: Calcium channel blockers; T2D: type 2 diabetes; ThAT vol: intrathoracic adipose tissue volume. **P<0.01 vs. no CAD. Continues variables expressed as means+/-SEM.

Table S4. Predictive value of FAI_{PVAT} to describe coronary artery disease and atherosclerotic plaque burden independently of Coronary Calcium Score

Independent variable	**Dependent variable**	
	R^2, P of the model	**(Standardized β, P)**
CAD	R^2= 0.657, P<0.0001	FAI_{PVAT} (β_{st}=0.074, P=0.01) ThAT volume (β_{st}=0.01, P=0.572) CCS (β_{st}=0.001, P=0.002) Smoking (β_{st}=0.570, P=0.202) Diabetes (β_{st}=0.701, P=0.277) Dyslipidemia (β_{st}=0.297, P=0.0001) Hypertension (β_{st}=0.863, P=0.051) Gender (β_{st}=0.834, P=0.109) Age (β_{st}=0.010, P=0.485)
Atherosclerotic plaque burden in RCA	R^2=0.337, P<0.0001	FAI_{PVAT} (β_{st}=0.565, P=0.0001) ThAT volume (β_{st}=0.212, P=0.0001) CCS_{RCA} (β_{st}=-0.067, P=0.299) Smoking (β_{st}=-0.095, P=0.130) Diabetes (β_{st}=0.080, P=0.190) Dyslipidemia (β_{st}=0.071, P=0.290) Hypertension (β_{st}=0.019, P=0.768) Gender (β_{st}=-0.008, P=0.902) Age (β_{st}=-0.012, P=0.485)

CAD: Coronary artery disease defined as stenosis >50% in any coronary artery; CCS: coronary calcium score; FAI_{PVAT}: Fat attenuation index in perivascular adipose tissue around the proximal right coronary artery; RCA: Right coronary artery; ThAT: intrathoracic adipose tissue